

# Author Manuscript

This is the author manuscript accepted for publication and has undergone full peer review but has not been through the copyediting, typesetting, pagination and proofreading process, which may lead to differences between this version and the [Version of Record](#). Please cite this article as [doi: 10.1111/GCB.15188](https://doi.org/10.1111/GCB.15188)

This article is protected by copyright. All rights reserved

# Allometric constraints and competition enable the simulation of size structure and carbon fluxes in a dynamic vegetation model of tropical forests (LM3PPA-TV)

Running Title: *A model of tropical forests for ESMs*

Isabel Martínez Cano<sup>1\*</sup>, Elena Shevliakova<sup>2</sup>, Sergey Malyshev<sup>2</sup>, S. Joseph Wright<sup>3</sup>, Matteo Detto<sup>1</sup>, Stephen W. Pacala<sup>1</sup> and Helene C. Muller-Landau<sup>3</sup>

<sup>1</sup>Department of Ecology and Evolutionary Biology, Princeton University, Princeton, NJ 08544, USA

<sup>2</sup> NOAA/Geophysical Fluid Dynamics Laboratory, 201 Forrestal Road, Princeton, NJ 08540, USA

<sup>3</sup>Smithsonian Tropical Research Institute, Box 0843-03092, Balboa, Ancón, Panamá

Correspondence to: Isabel Martínez Cano ([isamcano@gmail.com](mailto:isamcano@gmail.com))

## Abstract

Tropical forests are a key determinant of the functioning of the Earth system, but remain a major source of uncertainty in carbon cycle models and climate change projections. In this study, we present an updated land model (LM3PPA-TV) to improve the representation of tropical forest structure and dynamics in Earth system models (ESMs). The development and parameterization of LM3PPA-TV drew on extensive datasets on tropical tree traits and long-term field censuses from Barro Colorado Island (BCI), Panama. The model defines a new plant functional type (PFT) based on the characteristics of shade-tolerant, tropical tree species, implements a new growth allocation scheme based on realistic tree allometries, incorporates hydraulic constraints on biomass accumulation, and features a new compartment for tree branches and branch fall dynamics. Simulation experiments reproduced observed diurnal and seasonal patterns in stand-level carbon and water fluxes, as well as mean canopy and understory tree growth rates, tree size distributions, and stand-level biomass on BCI. Simulations at multiple sites captured considerable variation in biomass and size structure across the tropical forest biome, including observed responses to precipitation and temperature. Model experiments suggested a major role of water limitation in controlling geographical variation forest biomass and structure. However, the failure to simulate tropical forests under extreme conditions and the systematic underestimation of forest biomass in Paleotropical locations highlighted the need to incorporate variation in hydraulic traits and multiple PFTs that capture the distinct floristic composition across tropical domains. The continued pressure on tropical forests from global change

demands models which are able to simulate alternative successional pathways and their pace to recovery. LM3PPA-TV provides a tool to investigate geographic variation in tropical forests and a benchmark to continue improving the representation of tropical forests dynamics and their carbon storage potential in ESMs.

Keywords: *Barro Colorado Island; Carbon cycle; Earth system models; Forest production; LM3PPA-TV; Tropical forest*

## 1. Introduction

Tropical forests are a key determinant of the functioning of the Earth system. Tropical forests account for half of the carbon stored by plants and more than a third of the annual carbon uptake by the terrestrial biosphere (Chapin et al. 2011; Pan et al. 2013). This high productivity pumps water vapor through transpiration that cools the global atmosphere ( $\sim 0.5$  K over land, Snyder 2010), and represents a major sink for anthropogenic  $\text{CO}_2$  emissions that buffers climate change ( $\sim 0.15$  Pg C  $\text{yr}^{-1}$ , Le Quéré et al. 2018). However, the sustained provision of these ecosystem services depends on the resilience of tropical forests to global change. During this century, tropical forests will face warmer and drier conditions in a  $\text{CO}_2$  enriched atmosphere, and the continued pressure of deforestation (Lawrence and Vandecar 2015). These threats pose a critical challenge to anticipate changes in the structure and functioning of tropical forests and to elucidate potential feedbacks on the Earth system (Bonan 2016).

The assessment of tolerable stress levels and alternative mitigation strategies to limit the impacts of global change increasingly depends on Earth system models (ESMs). In the terrestrial domain, these models feature complex feedback loops between the climate system and changes in land cover through the explicit representation of vegetation processes on a range of temporal and spatial scales (Bonan 2008a,b). However, although ESMs capture large-scale gradients in plant production and emergent patterns like the distribution of biomes, the characterization of tropical forests remains a major source of uncertainty (Schimel et al. 2014). Predictions based on the current generation of ESMs diverge about whether tropical forests will become a net carbon source or remain as a sink in the near future (Friedlingstein et al. 2014 ; Cavaleri et al. 2015), and some ESMs even project the collapse of Amazon rainforests under dryer climate conditions at the end of the century (Drixfhout et al. 2015). These uncertainties highlight the need to improve the representation of tropical forests in ESMs through a more realistic implementation of ecological dynamics.

The current generation of ESMs include modules of varying complexity to enable the simulation of energy and material fluxes between land plants and the overlying atmosphere, the absorption of water and nutrients from the soil, and the decomposition of plant materials (Shevliakova et al. 2009; Fisher et al. 2018). These dynamic vegetation models (DVMs) can also feature different plant functional types (PFTs) to incorporate biogeographical changes in plant physiology and ecology associated with large-scale environmental gradients and historical contingency (Prentice et al. 1992). The same approach enables the simulation of human-altered landscapes and forest management actions like wood harvesting and reforestation (Hurtt et al. 2011). In the past, computational costs prevented an explicit representation of

1 important ecological aspects like changes in canopy structure or gap dynamics (Fisher et al. 2018).  
2 However, theoretical advances now provide efficient schemes to scale local forest dynamics to the large  
3 extents required to simulate the earth system in long-term simulations of climate change (Moorcroft et al.  
4 2001). Together with increasing availability of long-term studies and global compilations of species traits  
5 and forest measurements (Anderson-Teixeira et al. 2015, 2018; Falster et al. 2015; Schimel et al. 2015),  
6 these advances are boosting the development of improved DVMs.

7 Within the hierarchy of DVMs, the inclusion of detailed demographic processes and vertical canopy  
8 structure results in a more realistic representation of forest patch dynamics and ecosystem fluxes. These  
9 models inherit many of their characteristics from earlier forest gap dynamic simulators (Botkin et al. 1972;  
10 Shugart and West 1977; Pacala et al. 1996) but require a series of modifications to enable the simulation  
11 of forest dynamics at large scales (tens to hundreds of kilometers). Two alternative approaches prevail in  
12 the literature; the first method involves the simulation of a large number of individual trees within each  
13 ESM grid cell to average forest composition and associated fluxes (e.g., HYBRID, LPJ-GUESS, SEIB). The  
14 second approach, used in the present study, pursues the analytical upscaling of forest gap dynamics using  
15 integro-partial differential equations (ED, CLM(ED), Moorcroft et al. 2001). These analytical models  
16 approximate the dynamics of expected forest size structure and species composition by considering  
17 cohorts of identical individuals. The subsequent gain in efficiency allows a more detailed representation of  
18 processes like competition and succession. The heart of one such approach is the perfect plasticity  
19 approximation (PPA, Strigul et al. 2008), which enables an efficient implementation of the sequential  
20 partitioning of the light available for photosynthesis through the canopy. This approach has successfully  
21 reproduced successional dynamics in temperate forests (Purves et al. 2008, Weng et al. 2015), and the  
22 canopy structure and size distribution of tropical forests (Bohlman and Pacala 2012, Farrior et al. 2016).

23 Here, we present LM3PPA-TV, an updated version of the land model LM3-PPA (Weng et al. 2015) that  
24 features an improved representation of tropical vegetation in ESMs. Like its predecessor, LM3PPA-TV  
25 simulates vegetation dynamics by scaling plant physiological processes from cells and tissues up to the  
26 survival and reproduction of individual trees and the dynamics of plant populations at the landscape level.  
27 Height-structured competition for light and competition for water emerge from interactions among  
28 neighboring plants within a fully coupled model with dynamic soil hydrology and atmosphere. The new  
29 version of the model implements an updated growth allocation scheme based on realistic assumptions  
30 about tree size scaling, incorporates hydraulic constraints on stomatal control, and features a new  
31 compartment for tree branches and branch fall dynamics. The model also simulates disturbance and gap

recovery dynamics explicitly through the LM3 tiling scheme (Shevliakova et al. 2009; Milly et al. 2014), which allows the coexistence of tiles at different successional stages within the same grid cell.

The development and testing of the new LM3PPA-TV modules were guided by extensive analyses of global databases (Falster et al. 2015; Anderson-Teixeira et al. 2018) and of long-term monitoring and trait data available at Barro Colorado Island (BCI, Panamá, Hubbell et al. 2005; Wright et al. 2010). We defined a new plant functional type of shade-tolerant tropical tree, and tested the ability of the model to reproduce multiple vegetation patterns at BCI, from individual performance to ecosystem-level fluxes. Then, we extended the analysis to the global scale and evaluated model predictions against large-scale variation in forest biomass and size structure across the tropics.

## 2. Model description

LM3PPA-TV simulates vegetation dynamics by scaling photosynthetic reactions in leaves up to the survival and reproduction of individual trees within populations and the successional dynamics at the landscape level. Population dynamics and ecosystem patterns emerge from a mechanistic representation of the basic processes of tree growth, reproduction and mortality, and from differences in tree performance associated with competition for light and water resources. Importantly, vegetation modules are embedded in a much larger model, so the dynamic soil and atmosphere constrain physiological and tree-level processes. Here we provide an overview of model vegetation dynamics, including an introduction to the novel elements. Additional details on model vegetation dynamics including equations for plant physiological processes are given in the supplement.

### 2.1. Forest dynamics in LM3PPA-TV

As in LM3-PPA, the model represents forested areas within each grid cell by one or more tiles (§10.1). The number and relative area of tiles vary over time to represent heterogeneity in forest structure and implicitly capture the impact of disturbance and patch dynamics (see §2.3.2). The basic modelling units used to represent vegetation are cohorts each composed of identically sized individuals of a particular species or plant functional type (PFT) and are associated with a single tile. Each tile can contain multiple cohorts that compete for light and water, and thereby interact with one another. Cohorts from different tiles interact only indirectly through their impacts on atmospheric temperature and humidity at the grid cell scale.

The master equations of the model specify how the abundance  $N_i$  and the size  $s_i$  of trees in each cohort  $i$  vary through time;

$$\frac{dN_i}{dt} = -\mu[s_i, k_i, t] N_i \quad (1)$$

$$\frac{ds_i}{dt} = g[s_i, k_i, t] \quad (2)$$

where  $k_i$  is the canopy layer occupied by the individuals of cohort  $i$  at time  $t$  (see §2.1.1). The rates of mortality  $\mu$  and growth  $g$  vary through time as a function of tree size and canopy position, and with the dynamic environment experienced by each cohort, reflecting both changes in neighbor abundance that affect local resource availability, and changes in landscape composition that modulate local weather and climatic conditions.

Demographic dynamics are completed with the equation for recruitment of new cohorts in a tile which define the initial condition for eq. (1)

$$N_{i,0} = \int_{a_m}^{\infty} N(s, k, \tau) f_r(s, k, \tau) d\tau \quad (3)$$

where  $N_{i,0}$  is the initial density of seedlings of a predefined size  $s_0$  which populate a new cohort  $i$ . The integral is calculated locally for each tile and over all the trees with an age  $\tau$  above the age of maturity  $a_m$ . Per capita tree fecundity  $f_r$  varies with the size, canopy status, and cohort age, as detailed below (§2.3.1).

The equations above simplify the simulation of age and size structured vegetation dynamics by following the evolution of a discrete number of cohorts. This approach reduces the system to a set of ordinary differential equations and avoids the more complex –and potentially unstable– numerical schemes required to directly simulate changes in the distribution of cohort sizes and age structure (Weng et al. 2015).

### 2.1.1. Vegetation structure: assigning cohorts to canopy layers

Vegetation is represented as a set of cohorts composed of identical individuals that belong to a given species or plant functional type (PFT). Each cohort is characterized by the size and spatial density of its individual trees (number per unit ground area). Size is defined based on stem diameter and biomass. The model divides plant biomass into six tissues or dynamic carbon pools: labile nonstructural carbohydrates

(*NSC*), leaves (*L*), fine roots (*FR*), reproductive structures and propagules (*F*), sapwood (*SW*) and heartwood (*HW*).

Cohorts are arranged in vertical canopy layers according to the Perfect Plasticity Approximation (PPA, Strigul et al. 2008), a model featuring the sequential partitioning of the light available for photosynthesis based on the relative position of trees within the canopy. LM3PPA-TV implements a simplified PPA that assumes flat-topped crowns (Purves et al. 2008, Weng et al. 2015). Each cohort occupies a single canopy layer, and multiple cohorts can occupy the same layer (Fig. 1). The layer occupied by each cohort determines the amount of light received by its trees, setting up a competitive advantage for trees in the upper canopy layers relative to those in the lower layers. Trees in a given layer shade only trees in lower layers – i.e., they decrease the amount of light available for trees in all the layers beneath them. There is also self-shading among the leaves in the canopy of each tree (§10.3.2). Trees in the same layer are all assumed to have the same light incident on the top of their canopies (i.e., they do not shade each other).

In practice, the implementation of PPA starts with the ranking of individual cohorts based on the height of their trees, from tallest to smallest. Then, the canopy layer  $k_i$  occupied by a cohort  $i$  of trees with height  $H^*$  [m] is determined using the following definition:

$$k_i(H^*) = \int_{H^*}^{\infty} N_H A_C dH \setminus A_P \quad (4)$$

where  $N_H$  is tree density [individuals per meter of height],  $A_C$  is the crown area [m<sup>2</sup>] per tree of height  $H$ , and  $A_P$  is the area of the focal tile [m<sup>2</sup>]. The integral sums crown areas for all cohorts with trees taller than  $H^*$  within the same tile, and the integer division (indicated with the backslash symbol '\') floors the fractional number of layers to a zero-based layer index from the top of the canopy ( $k_i = 0$ ) to the understory ( $k_i = n_k - 1$ , where  $n_k$  is the total number of canopy layers).

The layer to which a given cohort is assigned is recalculated annually based on the cumulative canopy cover of all the trees taller than those in the target cohort. When this sum exceeds the area of the tile, the layer is closed and layer number  $k$  increases one unit. Thus, the model always includes a top canopy layer and, when cumulative cover exceeds the area of the tile, one or more understory layers that shade each other from the tallest to smallest. This process may require splitting individual cohorts between layers, since each cohort can belong only to a single layer. In this case, the resulting two new cohorts are assigned to different layers and start following independent trajectories.

## 2.2. Tree level dynamics

### 2.2.1. Tree allometry

Allometric functions provide a basic template to model changes in tree morphology and thus growth allocation with size. Two key dimensions for light competition were defined based on allometric functions of trunk diameter ( $D$  [m]): crown area and tree height. The form and parameterization of these allometric functions was based on an extensive analysis of species-specific tree morphological data from BCI (Martínez-Cano et al. 2019). The projected areal extent of the crown of each tree ( $A_C$  [m<sup>2</sup>]) was modelled as a power function of trunk diameter:

$$A_C(D) = a_C D^{b_C} \quad (5)$$

where the intercept  $a_C$  determines the baseline level and the exponent  $b_C$  the overall shape of the curve. Tree height ( $H$  [m]), defined as the height at the top of the crown, was modelled as a saturating function of trunk diameter using a generalized Michaelis-Menten function:

$$H(D) = \frac{a_H D^{b_H}}{k_H + D^{b_H}} \quad (6)$$

where  $a_H$  is the asymptotic tree height, and the exponent  $b_H$  and the inflection parameter  $k_H$  determine how fast tree height increases with diameter. Note that equation (6) features a deceleration in the rate of increase of tree height with trunk diameter. This relationship provides some advantages over alternative approaches featuring non-saturating allometric functions that can lead to the simulation of unrealistically tall trees (Weng et al. 2015).

The allometric relationship for tree height is also used to describe changes in woody biomass ( $B_W$  [kg of C]) using the allometric model parameterized by Chave et al. (2014) to describe size scaling of above-ground tree biomass in tropical forests:

$$B_W(D) = \alpha_{BM} \rho D^2 H \quad (7)$$

where  $\rho$  [kg m<sup>-3</sup>] is a species-specific estimate of wood density (dry mass per fresh volume, technically wood specific gravity), and  $\alpha_{BM}$  is a unitless parameter that accounts for tapering and for the fraction of woody biomass in branches. As detailed in §10.3.2, this equation can be inverted to translate the allocation of woody biomass into changes in aerial tree dimensions.

### 2.2.2. Allocation of assimilated carbon

Plant growth is modelled as a function of the biomass of assimilated, nonstructural carbon per tree ( $NSC$  [ $\text{kg C tree}^{-1}$ ]). In the model,  $NSC$  represents a labile component that acts as the currency for the allocation of biomass to the growth and maintenance of different plant tissues. The biomass of  $NSC$  is updated daily based on the balance between net carbon acquisition and investment:

$$dNSC/dt = NPP_d - G_d \quad (8)$$

where both the daily net primary production,  $NPP_d$  [ $\text{kg C tree}^{-1}\text{day}^{-1}$ ], and the daily growth rate,  $G_d$  [ $\text{kg C tree}^{-1}\text{day}^{-1}$ ], of each individual tree are themselves functions of the available  $NSC$  pool.

The balance between instantaneous photosynthetic carbon uptake ( $P_s$  [ $\text{kg C tree}^{-1}\text{s}^{-1}$ ]) and maintenance and growth respiratory losses ( $R_A$  [ $\text{kg C tree}^{-1}\text{s}^{-1}$ ]) is integrated to calculate daily net primary production:

$$NPP_d = \int_0^{d_s} (P_s - R_A - f_E \cdot \max\{0.0, P_s - R_A\}) dt \quad (9)$$

where  $f_E$  is the fraction of instantaneous  $NPP$  allocated to root exudates and  $d_s$  is day length in seconds (the integrand was updated every half hour in the simulations reported here). Because nutrient uptake is not explicitly represented in the current model, root exudates act as a passive carbon sink (see Sulman et al. 2019 for LM3 extensions featuring interactive nutrient dynamics). The truncation in the last term of eq. (9) ensures that no structural carbon is mobilized to release root exudates when the balance between production and respiration is negative. See §10.3 for a detailed account of plant energy and material fluxes, including the new module implementing hydraulic constraints on stomatal control (Wolf et al. 2016, §10.3.3).

Individual daily growth ( $G_d$  [ $\text{kg C tree}^{-1}\text{day}^{-1}$ ]) depends on available  $NSC$  and consists of the production of new leaves ( $L$ ), fine roots ( $FR$ ), branches ( $BR$ ) and other structural wood ( $W$ ), and reproductive tissues and seeds ( $F$ ):

$$G_d = G_L + G_{FR} + G_{BR} + G_W + G_F. \quad (10)$$

All the growth rate components are nonnegative for an actively growing tree. Allocation of resources to the growth of each major tissue depends on a series of targets that define allometric constraints on the morphology and anatomy of simulated trees (Weng et al. 2015). These dynamic targets vary depending on tree size, phenological status and position within the canopy. Trees adjust growth rates of different compartments to minimize deviations from targets (see §10.2 for a detailed description).

The net accumulation of new biomass for each individual tree results from the balance between carbon allocated during growth and losses associated with tissue turnover. The model implements tissue turnover as a constant rate process affecting the biomass of leaves, fine roots and branches according to a set of turnover rates specific for each of these tissues ( $\alpha_i$ , Table S1). Together with decomposing tissues from dead individuals and failed seeds, tissue turnover results in a net flux of carbon to the soil (Shevliakova et al., 2009). Importantly, LM3PPA-TV introduced a new sapwood compartment for branches (see §10.2) to implement carbon fluxes due to branchfall (Palace et al. 2008; Marvin and Asner 2016) and to slow tree biomass accumulation.

## 2.3. Demographic processes

### 2.3.1. Tree fecundity and recruitment

The model implements the recruitment of new seedlings to the population as a discrete annual event, synchronized across all reproductive trees, that is the culmination of sustained investment in the production and maintenance of reproductive tissues ( $F$ ). Trees allocate resources to reproduction ( $G_F > 0$ ) only if they survive beyond the age of maturity ( $a_m[years]$ ), and are in the top canopy layer; otherwise, they remain in a non-reproductive state ( $G_F = 0$ ; see eq. 26 in §10.2). Reproductive allocation cumulates on a daily basis during the time span  $t_R$  (here 1 year) between two successive reproductive events.

The overall fecundity per tree in a given cohort,  $f_r$ , is defined as the number of seedlings produced by each tree that reach establishment:

$$f_r = p_g p_e \frac{F_{t_R}}{B_S} = p_g p_e \frac{1}{B_S} \int_0^{t_R} G_F dt \quad (11)$$

where the cumulated reproductive biomass at the time of reproduction ( $F_{t_R}$ ) is partitioned into seedlings each having initial biomass  $B_S$ . The value of  $B_S$  is inverted from biomass allometry to ensure that seedlings recruit at an initial height of 10 cm. Recruitment success further depends on the probabilities of germination  $p_g$  and initial establishment  $p_e$ , although there are other sources of early mortality (e.g. carbon starvation; see below). Failed seedlings contribute a net carbon flux to the soil.

### 2.3.2. Mortality and disturbance

LM3PPA-TV implements three mortality mechanisms that decrease the density of affected cohorts: carbon starvation, background mortality, and gap-associated mortality. Carbon starvation mortality operates at the daily scale: individuals die if plant reserves fall below a minimum threshold ( $NSC$  pool less than 1% of the target leaf biomass,  $L^*$ ) or if their sapwood biomass drops to zero. In practice, this source of mortality most often affects seedlings and saplings in the lower canopy layers, and thus constitutes an emergent mechanism of density-dependent regulation.

Background mortality accounts for most other sources of mortality that are not explicitly implemented in the model, including wind throw, lightning, and disease. This mechanism features density-independent mortality associated with unpredictable fatalities, although it was implemented as a deterministic constant decay process operating at the annual scale at a rate that varies between canopy and understory trees and among PFTs (Table S2). Background mortality rates,  $\mu$ , are assumed to be size-independent for canopy trees,  $\mu_c(D) = \bar{\mu}_c$  [year<sup>-1</sup>], and to decrease asymptotically with size for understory trees (Weng et al. 2015):

$$\mu_u(D) = \bar{\mu}_u \frac{1 + a_{mort} \exp\{-b_{mort} (D - D_0)\}}{1 + \exp\{-b_{mort} (D - D_0)\}} \quad (12)$$

where  $\bar{\mu}_u$  [year<sup>-1</sup>] is a species-specific parameter corresponding to the background mortality rate of understory trees,  $a_{mort}$  [–] and  $b_{mort}$  [m<sup>-1</sup>] are constants that determine the shape of the mortality curve and  $D_0$  [m] is stem diameter at germination. For  $a_{mort} = 4.0$  as here, this leads to a decrease in background understory mortality rates by a factor  $\frac{1}{2}(1 + a_{mort}) \approx 2.5$  from establishment to 25 cm diameter. Mortality parameters  $\bar{\mu}_c$  and  $\bar{\mu}_u$  were estimated based on tree survival in the forest dynamic plot at BCI (see §10.4, Table S2).

Annual background mortality of canopy trees is also associated with the generation of forest gaps following a disturbance. In tiles where vegetation is structured in more than one layer, the death of canopy trees triggers the formation of gaps with a reduced density of individuals and with marked differences in size structure. The model implements this mechanism taking advantage of the tiling scheme for land use and subgrid-scale heterogeneity as in previous versions of the Land Model (Shevliakova et al. 2009; Milly et al. 2014).

A tile affected by canopy tree death is split into two tiles; one is a new forest gap with an area equivalent to the total crown area of canopy trees that died, while the other covers the remaining area and preserves

forest structure before the disturbance, that is, an equal proportion of all the cohorts that inhabited the original tile (Fig. S2). The freshly formed forest gap tile only keeps trees in the understory that can additionally survive gap-associated, size-independent mortality ( $\mu_u^g$ , here equal to 0.9 per gap formation event), intended to represent mortality due to damage from the fall of the canopy trees that died and from changed environmental conditions in the newly opened gap. The removal of trees in the newly formed gap tile provides the surviving trees with easier access to sunlight and water, potentially changing their fate and dynamics.

### 3. Model parameterization

Our strategy for model parameterization was hierarchical and structured in three stages. First, we reviewed the literature to identify parameters that are well constrained by direct experimental and field measurements and are relatively invariant across species. In most cases, these parameters describe the rates and thermal sensitivities of biochemical reactions and physiological processes associated with plant metabolic processes. Except when noted, these parameters were regarded as fundamental constants within the model.

The second category of parameters involved quantities that show extensive variation among species and whose mean value can be estimated based on available data for tropical forests. The majority of these parameters relate to the morphology of simulated trees, including the allocation of assimilated carbon to different tissues. For instance, we assumed that the target for the investment in the growth of new branches was determined by the fraction of woody biomass in branches,  $p_{BR}$ , which was set as the average of all measurements available for tropical tree species in the Biomass And Allometry Database (BAAD, Falster et al. 2015). In other cases, the precise value of a parameter was inverted to match well-established allometric relationships across species. For instance, the conversion from sapwood to heartwood depends on a quantity,  $\varphi_{ASW}$ , that varies depending on the scaling of tree height and crown area with trunk diameter (eq. 35, §10.2). Thus, we constrained  $\varphi_{ASW}$  to match the observed relationship between sapwood area and trunk diameter across different tree species at BCI (Meinzer et al. 2001). These parameters enter the model as idealized values that guide changes in tree growth and allocation patterns for trees under different environmental conditions. Although setting these parameters as constants is seemingly at odds with observed variability in the field, combining data from multiple species enables confident estimates of overall mean values.

The third category of parameters involved quantities that have hardly been studied and thus remain highly uncertain. In this case, we took advantage of the model to determine suitable values depending on their ability to produce realistic NPP rates and stand-level biomass patterns. For instance, the ratio of total root surface area to the total leaf area,  $\phi_{RL}$ , was tuned to match stand-level fine root biomass densities observed at BCI (Wurzburger and Wright 2015). Parameter tuning did not involve the set of emergent patterns used to assess model quality (i.e., individual tree growth rates, diurnal and seasonal cycles of photosynthesis and evapotranspiration, and tree size distributions), ensuring the independence among the data used to tune model parameters and the data used to assess model fit. Table S1 in the online supplement provides a complete list of model variables and parameters.

#### 4. Experimental design and simulations

##### 4.1. Forest dynamics at BCI

The first set of model experiments used as a test bed the tropical moist forest located at Barro Colorado Island (BCI, Panama). This benchmark location provides abundant information to parameterize and evaluate the model, including microclimatic, physiological, morphological and demographic data recorded since 1923 (Leigh 1999), and especially, following the establishment of the 50-ha forest monitoring plot in 1981 (Condit 1998; Hubbell et al. 1999; 2005). These data enabled the definition of the PFT and the assessment of vegetation patterns from individuals to the ecosystem scale. The model was run in a single cell, centered at 79.5 °W, 9.5°N, with flat topography and no water bodies. Simulations started by planting one monoculture cohort of seedlings in a single tile homogeneously covered by bare soil. Tile splitting remained active during the entire simulation to allow the coexistence of forest tiles with different characteristics within the model cell (see §2.3.2).

The simulations featured alternative parameterizations of the single PFT based on the characteristics of four shade-tolerant canopy species. Specifically, the parameterizations were based on functional traits and performance measures recorded at BCI for *Beilschmiedia pendula*, *Brosimum alicastrum*, *Prioria copaifera*, and *Quararibea asterolepis*. These species are locally abundant (relative abundance in terms of % basal area > 1.9%) and they are representative of the variation in allometric scaling and in demographic rates observed for shade-tolerant tree species at BCI. Alternative PFT parameterizations assumed that species were identical except for canopy and understory background mortality rates, the allometric scaling of tree height and crown area, wood density and LMA (Table S2). Species-specific functional traits and performance measures were retrieved from BCI databases and from dedicated analyses based on BCI

census data (see §10.4 and Table S2 for further details). Model performance was evaluated in terms of the ability to reproduce patterns observed in remote sensing, eddy covariance, tree census, and litterfall data collected locally and in other tropical forests.

#### 4.2. Large-scale patterns in biomass and size structure

In a second set of experiments, the model was evaluated at multiple locations across the tropics to examine its ability to reproduce large-scale gradients in forest biomass and size structure. First, we used as a reference the set of stand level estimates of above ground biomass (AGB,  $\text{Kg C m}^{-2}$ ) available in the global Forest Carbon database, *ForC* (Anderson-Teixeira et al. 2018). We simulated forest dynamics for the subset of *ForC* plots covered by mature (age > 100 years), intact tropical forests. Each plot was assigned to the nearest  $1^\circ \times 1^\circ$  cell of a regular grid with origin at  $179.5^\circ\text{W } 89.5^\circ\text{N}$  (cell center) in order to extract the corresponding average meteorological conditions over the cell from Sheffield et al. (2006) forcing data set (see below). In cases in which multiple plots were located in the same grid cell, we used the average AGB as a reference. In a second set of model simulations, we examined changes in forest size structure across the tropics. We compared LM3PPA-TV predictions with observed size structure at the forest plots analyzed by Muller-Landau et al. (2006).

#### 4.3. Boundary conditions and meteorological forcing

Weather conditions varied during each simulation to account for diurnal, seasonal and multiannual impacts of meteorological forcing and climatic variability on vegetation dynamics. We relied on the 3-h atmospheric reanalysis fields from Sheffield et al. (2006) forcing dataset, which is available for the period 1948-2010. The dataset uses a variety of observations to amend known biases in the NCEP/NCAR atmospheric reanalysis (Kalnay et al. 1996). Forcing data includes downward long- and short-wave radiation [ $\text{W m}^{-2}$ ], surface pressure [Pa] and wind speed [ $\text{m s}^{-1}$ ], precipitation [ $\text{Kg m}^{-2} \text{s}^{-1}$ ], 2 m air temperature [K], and specific humidity [ $\text{kg kg}^{-1}$ ]. We ran each simulation in a 20 year loop (1951-1971) using the Sheffield et al. (2006) forcing data at each target location. With this approach, we avoided long-term trends associated with climate warming while retaining multiannual variation due to irregularly periodic climate phenomena such as El Niño Southern Oscillation (ENSO, McPhaden et al. 2006). All experiments assumed a constant  $\text{CO}_2$  concentration,  $[\text{CO}_2] = 350 \text{ ppm}$ .

## 5. Results

### 5.1. Forest dynamics at BCI

The assessment of LM3PPA-TV at BCI relied on a series of monoculture experiments simulating the colonization of an empty gap following a perturbation. The model converged in approximately 200 years to an equilibrium above ground biomass density (AGB) of 16.48 [14.95, 17.65]<sub>90%</sub> kg C m<sup>-2</sup> (mean and 90% central quantile interval for the last 100 years of a 500-year simulation). As the forest patch matured, the initial accumulation of biomass was accompanied by an overshoot in total abundance that settled through self-thinning towards an equilibrium density of 395 individuals per ha greater than 10 cm in diameter (compared with an observed average of 430, for 1982-2015, Rutishauser et al. 2020). The forest rapidly structured into three layers, with the top canopy layer accounting for 66.5% of total forest biomass. Mean leaf area index (LAI) in the model was 8.20 m<sup>2</sup> of leaf per m<sup>2</sup> of ground, which falls at the higher end of available field estimates (5.4-8.4; see Discussion for further details).

Carbon fixation in the forest added up to an average gross primary production (GPP) of 2.99 [1.88, 3.49]<sub>90%</sub> kg C m<sup>-2</sup> yr<sup>-1</sup> (Fig. 2), close to mean GPP estimates based on BCI eddy covariance data for July 2012 to August 2017 (2.7 kg C m<sup>-2</sup> yr<sup>-1</sup>), and within the range of tropical forest GPP estimates in the *ForC* database (mean 3.27 [2.87, 3.89]<sub>90%</sub> kg of C m<sup>-2</sup> yr<sup>-1</sup>,  $n = 25$ ; Anderson-Teixeira et al. 2018). Around 60% of GPP was devoted to autotrophic respiration to leave a net primary production (NPP) of 1.24 [0.33, 1.67]<sub>90%</sub> kg C m<sup>-2</sup> yr<sup>-1</sup> (Fig. 3). NPP predictions compared well with independent estimates for BCI based on satellite-derived radiation absorption by plants (1.16 [0.85, 1.85]<sub>90%</sub> kg C m<sup>-2</sup> yr<sup>-1</sup>, average of MODIS values for the period 2000-2014, Running et al. 2015) and with plot-based tropical NPP estimates from *ForC* (1.17 [0.85, 1.61]<sub>90%</sub> kg C m<sup>-2</sup> yr<sup>-1</sup>,  $n = 18$ ). The model predicted that approximately half of annual NPP is devoted to wood production (0.68 [0.52, 0.83]<sub>90%</sub> kg C m<sup>-2</sup> yr<sup>-1</sup>, Fig. 3), of which one quarter corresponds to branch production to compensate branch turnover (26.5% [22.0, 32.0]<sub>90%</sub>). Thus, wood production less branchfall is estimated at 0.425 kg C m<sup>-2</sup> yr<sup>-1</sup>, which compares with an average of 0.372 kg C m<sup>-2</sup> yr<sup>-1</sup> estimated by Meakem et al. (2018, their Table S2) from BCI forest plot data for 1990-2010. Modelled leaf litterfall averages 0.34 kg C m<sup>-2</sup> yr<sup>-1</sup>, compared with the observed average of 0.32 kg C m<sup>-2</sup> yr<sup>-1</sup> for the BCI 50 ha plot (S. J. Wright, unpublished data).

Diurnal production and respiration cycles varied seasonally (Fig. 4). During the wet season, production tracked light availability with an average peak at noon at 24.2 [24.1, 25.5]<sub>50%</sub> μmol CO<sub>2</sub> m<sup>-2</sup> s<sup>-1</sup> (slightly above the eddy covariance average of 22.9 μmol CO<sub>2</sub> m<sup>-2</sup> s<sup>-1</sup>). In the dry season, GPP diurnal cycles showed an early peak (~2h before noon) and a depressed maximum of 18.1 [12.9, 23.4]<sub>50%</sub> μmol CO<sub>2</sub> m<sup>-2</sup>

1  $s^{-1}$  (below the  $20.4 \mu\text{mol CO}_2 \text{ m}^{-2} \text{ s}^{-1}$  from eddy covariance data). Average daily gross production was 21%  
2 lower during the dry season ( $6.8$  vs.  $8.6 \mu\text{mol CO}_2 \text{ m}^{-2} \text{ s}^{-1}$ , Fig. 4), although stomatal water loss accounted  
3 for a higher proportion of evapotranspiration (77 vs. 58%). As a consequence, average ET rates remained  
4 comparable between the dry and the wet season ( $91.4$  vs  $98.3 \text{ W m}^{-2}$ ), and resulted in an annual average  
5 ET of  $96.2 [93.3, 99.9]_{50\%} \text{ W m}^{-2}$ .

6 To assess the reliability of ecosystem level estimates based on LM3PPA-TV simulations, we further  
7 evaluated model predictions at the individual and population levels. Annual growth patterns in LM3PPA-  
8 TV captured the marked contrast in production between canopy and understory trees (Fig. 5). Average  
9 annual trunk diameter increments for canopy trees growing at full light were similar to those observed  
10 ( $5.61 [4.00, 7.35]_{90\%}$  for the model vs. the observed  $5.13 [0.34, 12.48]_{90\%} \text{ mm yr}^{-1}$ ), even if modeled  
11 distributions were less variable than observations. In the case of understory trees, the model captured the  
12 positive skewed distribution of annual growth rates, albeit mean growth rates were higher than field  
13 estimates ( $0.83 [0.22, 2.11]_{90\%}$  vs. the observed  $0.69 [0.20, 2.02]_{90\%} \text{ mm yr}^{-1}$ ).

14 Background mortality and gap formation patterns in the model were prescribed. In contrast, carbon  
15 starvation represents an emergent mortality mechanism that was the main cause of early mortality in  
16 lower canopy layers and accounted for up to  $\sim 90\%$  of the mortality of small-sized individuals ( $D < 10 \text{ cm}$ ;  
17 mainly recently recruited seedlings). Mortality by carbon starvation varied among years paralleling  
18 changes in water availability and lowered GPP rates during the dry season. Similarly, interannual  
19 fluctuations in recruitment success reflected variation in seed production ( $31$  vs  $24 \text{ g C m}^{-2}$  in wet and dry  
20 years defined by the sign of annual precipitation anomalies, respectively); but note that Detto et al. (2018)  
21 found the opposite pattern using seed trap data. Observed reproductive litterfall averaged considerably  
22 higher, at  $96 (\text{SD } 19) \text{ g C m}^{-2}$  (S. J. Wright, unpublished data).

23 Together, simulated growth, recruitment and mortality patterns in LM3PPA-TV resulted in a realistic size  
24 distribution that resembled the spectrum observed in the field (Fig. 6). The model predicted a size  
25 distribution consistent with a broken power law scaling (e.g., Farrior et al. 2016). Smaller size classes up to  
26 a diameter of  $\sim 75 \text{ cm}$  consisted of understory individuals whose abundance declined by  $\sim 3/4$  per 10%  
27 increase in diameter (power law exponent  $b = 2.75$ , very close to the estimate of 2.84 for trees above 20  
28 cm reported by Muller-Landau et al. 2006). Larger size classes were less crowded, and the decline in  
29 abundance became more pronounced due to enhanced growth rates in the canopy as the scaling of the  
30 size spectra transitioned to an exponential distribution (defined by the parameter  $\lambda = 4.59$ ).

The assessment revealed a moderate sensitivity of the model to alternative parameterizations of the tropical tree PFT. Ecosystem level fluxes were robust to the choice of the shade-tolerant BCI species used to parameterize the PFT, with small variations in GPP and NPP among monoculture runs (Fig. S4). Other patterns like the overall carbon accumulated in wood varied depending on canopy mortality rates and tree allometry. For instance, equilibrium AGB increased by a factor of ~1.5 in monoculture runs featuring the PFT parameterization based on *Prioria copaifera*; its low canopy mortality rate lead to the accumulation of a high density of large canopy trees (Fig. 6, Table S2).

## 5.2. Large-scale patterns in biomass and size structure

LM3PPA-TV simulations forced under realistic weather conditions for 162 tropical sites resulted in one order of magnitude variation in AGB (Fig. 7). Model predictions of AGB were well-correlated with observed values (Pearson  $r = 0.4$ ), with a mean absolute deviation of 5.5 kg C m<sup>-2</sup>. However, LM3PPA-TV was unable to simulate the extreme AGB values observed at some paleotropical locations (median and range AGB of 17.2 [1.0, 24.4]<sub>Rg</sub> vs 15.4 [2.1, 36.7]<sub>Rg</sub> kg C m<sup>-2</sup> for simulated and observed, respectively). There was an overall trend towards underestimation of AGB in the Paleotropics (mean bias -5.4 [-8.5, -1.2]<sub>50%</sub> kg C m<sup>-2</sup>), and slight over estimation in the Neotropics (+1.0 [-3.0, 5.3]<sub>50%</sub> kg C m<sup>-2</sup>).

To better understand the emergence of large-scale gradients in biomass, we explored the relationships of observed and simulated AGB with mean annual temperature and mean annual precipitation in the forcing datasets. In the model, among-site variation in forest biomass mainly reflects changes in water availability, with a neat saturating relationship between simulated AGB and annual precipitation (Fig. S5). The same relationship was much weaker in the forest plot data and suggested instead a unimodal relationship with a peak in AGB at ~2200 mm yr<sup>-1</sup> (Fig. S5). The relationship with annual mean temperature was unimodal both in model predictions and in observations, with a suggestion of a peak at ~24 °C (Fig. S5).

We further explored whether the simulation of realistic gradients in forest biomass reflected the ability of the model to capture changes in size structure across the tropics. Overall, there was qualitatively good agreement between LM3PPA-TV simulations and observed size structure across a set of locations spanning a gradient from wet to dry conditions (Fig. 8). The model captured variability in the abundance of different size classes, from the consistent smooth decay of abundance with size in humid forests (e.g., Sinharaja), to the sharp truncation of size structure due to the lack of large trees in dry forests (Mudumalai). However, model predictions deviated from observed abundances at large size classes, especially in dry locations,

where the truncation of size structures at comparatively small diameters resulted in the underestimation of tree abundance (Ituri-Edoro and Ituri-Lenda) or even prevented the simulation of viable forest (HKK Wildlife Sanctuary, not shown in Fig. 8).

## 6. Discussion

### 6.1. Evaluating model performance at BCI

The core development of LM3PPA-TV built on more than three decades of field research at Barro Colorado Island (BCI, Hubbell et al. 2005; Wright et al. 2010). This empirical effort informed the development and parameterization of an updated dynamic growth allocation scheme that was fundamental for the emergence of realistic ecosystem properties. Model-based estimates were within 20% of either satellite or ground-based estimates of forest production and biomass, and they resulted in a realistic size structure that mirrored the size spectra retrieved from forest plot inventories, which represents a remarkable achievement for a model of these characteristics (Fisher et al. 2018).

In the model, the tree size distribution emerges from a complex interplay among changes in growth and demographic rates that depend on tree size and canopy position (Bohlman and Pacala 2012; Farrior et al. 2016). The model implements a competitive advantage for large trees growing in the sun that is countered by structural limits to height growth (Muller-Landau et al. 2006). The explicit simulation of gap dynamics through the land tiling scheme, which is another distinctive feature of the ED (Moorcroft et al. 2001) and LM family of models (Shevliakova et al. 2009; Milly et al. 2014), enabled the model to implicitly capture the distribution of patch ages and thereby contributed to the production of realistic tree size distributions. Together with the inclusion of tree height saturation, the new growth scheme improved the balance between biomass accumulation and losses and thereby suppressed the accumulation of extremely large trees in simulated forests, which are known to bias both forest structure and production estimates in other models – the so called big tree problem (Weng et al. 2015; Koven et al. 2019).

Modeled tree growth rates were comparable to those observed in the field, reflecting a consistent balance between net production (well constrained by physiological parameters) and allocation to other compartments, notably reproduction and compensation for branch turnover. LM3PPA-TV introduced a new sapwood compartment to enable the turnover of branches that, due to a lack of direct measurements, was assumed to be a constant value of  $0.05 \text{ yr}^{-1}$ . This translated into a predicted branch fall that accounts for a quarter of the total woody debris flux on BCI, a figure within the range observed in

the tropics (16-47%, Palace et al. 2008; Malhi et al. 2014; Marvin and Asner 2016), but above available estimates for BCI (Gora et al. 2019). Model predictions may also be sensitive to other poorly constrained processes like stem respiration, reproduction, and the production of root exudates, highlighting the need for continued observations to further constrain carbon fluxes in tropical forests. Importantly, real tree growth rates are also reduced by liana infestation (Ingwell et al. 2010), which is not currently represented in the model.

The model overpredicted leaf area index (LAI) in comparison with most other available estimates, albeit we lack direct measurements of this quantity for this site. The model predicted average LAI of 8.2 is higher than indirect estimates available at BCI based on locally collected optical methods (5.4 [3.0-8.0] (mean and range) by Wirth et al. (2001) and 5.9 [5.0-6.6] estimated by Detto et al. (2015, 2018)) or remote sensing data (e.g., MODIS LAI is always below 7.0), but showed better agreement with the allometric estimate of 7.25 by Leigh (1999) or the optical measurements of Mora et al. (2014) ( $8.4 \pm 1.2$ ; mean  $\pm$  SD). To our knowledge, the only direct measurement of LAI available for a tropical landscape, obtained using destructive sampling methods, was conducted by Clark et al. (2008) in a wet tropical forest in Costa Rica. They observed an average LAI of 6.00 [1.2-13.0], in good agreement with MODIS estimates of 6.10 for that site. An obvious explanation for the relatively high LAI values simulated by LM3PPA-TV lies in the choice of a target LAI\* of 6.0 for canopy trees. This value is based on direct LAI measurements on individual trees of shade-tolerant species taken at the Metropolitan Natural Park of Panama, close to BCI (Kitajima et al. 2005). Setting a lower target (LAI\* = 4) decreases modeled LAI to 6.49 [5.99-7.10] and increases the mean number of canopy layers from 2.9 to 3.8; in better agreement with the 4 layers estimated at BCI by Bohlman and Pacala (2012). However, this also increased AGB from 16.5 to 20.3 kg C m<sup>-2</sup>, well above available estimates for BCI (Martínez-Cano et al. 2019). Given the divergence of different indirect LAI estimates, there is a clear need for more direct sampling of LAI to evaluate and calibrate indirect estimates (Fang et al. 2019).

## 6.2. Large scale patterns in tropical forest biomass and size structure

The ability of LM3PPA-TV monoculture experiments to capture a substantial fraction of large-scale variation in tropical forest biomass and size structure highlighted the robustness of the parameterization developed for BCI. This set of results reinforces the transferability of the model and its consistency under a range of disparate environmental conditions, with reliable AGB and size structure predictions from dry to wet forests covering a variety of forest types (from tropical deciduous and semi-deciduous forest to

1 evergreen, tropical rainforests). These experiments demonstrated a leading role for external  
2 environmental forcing in driving large-scale variation in forest biomass and size structure across the  
3 tropics and, more specifically, the sensitivity of model predictions to changes in water availability. This is  
4 consistent with empirical analyses (e.g., Becknell et al. 2012, Lewis et al. 2013, Vilanova et al. 2018) as well  
5 as results from other models (e.g., Levine et al. 2016; Longo et al. 2019a,b). However, model simulations  
6 deviated substantially from observations under dry conditions and even failed to produce viable forests in  
7 locations with very low precipitation (i.e., 1000 mm per year). This highlights the need to implement  
8 multiple PFTs varying in hydraulic traits, and enable the emergence of variation in functional composition  
9 across sites and over time (Levine et al. 2016; Xu et al. 2016; Powell et al. 2018; Longo et al. 2019 a,b).

10 Although LM3PPA-TV captured overall gradients in forest biomass with precipitation and temperature, it  
11 presented a structural bias between the two major tropical ecozones. There was a trend towards the slight  
12 overestimation of forest biomass in the Neotropics (Central, South American, and Caribbean) and  
13 substantial underestimation of forest biomass in the Paleotropics (Africa, Asia and Australia). The relatively  
14 minor overestimation in Neotropical sites could easily be ascribed to local conditions unaccounted by the  
15 model (e.g., effects of soil fertility, Lloyd et al. 2015, Wright 2019; local topography, Muscarella et al. 2019).  
16 However, these explanations seem inadequate to explain the large underestimation of forest biomass in  
17 the Paleotropics and the inability to simulate the extreme AGB values that confer this ecozone a  
18 disproportionate importance for carbon storage at the global scale (Taylor et al. 2019). These biases likely  
19 reflect the need to consider multiple, geographically restricted PFTs to capture biogeographic differences  
20 in floristic composition across the tropics (Slik et al. 2018), like the prevalence of tall-statured, high-  
21 biomass species in the Paleotropics (Feldpausch et al. 2011; Banin et al. 2012; Taylor et al. 2019).

22 Taken together, these results reinforce the need for at least two distinct sets of functional groups to  
23 reflect biogeographic effects on the functioning of tropical forests and their response to large-scale  
24 gradients in climatic forcing. Future extension of LM3PPA-TV to simulate multiple tropical tree PFTs  
25 simultaneously provides a strong framework to test alternative hypotheses and advance towards a  
26 mechanistic understanding of the emergence of large-scale gradients in forest biomass and size structure  
27 with respect to changes in demographic, allometric and hydraulic traits. This aligns with similar efforts that  
28 strive to balance model complexity with a sufficient representation of functional diversity to achieve  
29 realistic forest successional pathways and ecosystem fluxes across sites (e.g., Levine et al. 2016, Fyllas et al.  
30 2017, Marechaux and Chave 2017, Powell et al. 2018, Longo et al. 2019a,b, Koven et al. 2019).

### 6.3. Current limitations and directions for future research

The ability of LM3PPA-TV monoculture experiments to capture basic characteristics of the BCI forest and considerable large-scale variation in tropical forest biomass and size structure provides a benchmark to continue improving the representation of tropical vegetation dynamics in ESMs. A next step is a full-scale assessment of the transferability and scalability of LM3PPA-TV to the regional and global scales targeted by ESMs. The ability of the model to reproduce large-scale variation in stand biomass and tree size distributions is encouraging, but many more patterns remain to be evaluated. We anticipate that adding additional PFTs capturing variation in plant allometry and hydraulic traits within and across tropical biomes would further improve overall model performance at these scales, but this remains to be tested.

There is also considerable scope for further improving the structure of LM3PPA-TV. One area for model improvement is the representation of mortality. Although the model implements demographic processes at the individual level, it lacks a mechanistic representation for mortality except in the case of carbon starvation (Weng et al. 2015). Background mortality and gap formation are parameterized as constant processes that depend only on tree canopy position (e.g. Johnson et al. 2018). The implementation of additional mortality mechanisms requires detailed knowledge about different sources of mortality, from the impact of weather extremes and fires to losses due to lianas and biotic agents. Unfortunately, our understanding of tropical tree mortality processes remains limited, hampering our ability to implement these mechanistically in models (McDowell et al. 2018).

Another aspect that requires further analysis and development involves the characterization of plastic responses to seasonal and interannual variation in environmental conditions (Abernethy et al. 2018; Sakai and Kitajima 2019). There is mounting evidence that tropical trees modify their photosynthetic apparatus and other leaf traits, and alter reproductive strategies in response to changes in light, water availability and temperature (Wright and Schaik 1994; Wu et al. 2016, 2017). These responses have been linked to changes in water fluxes between the dry and wet season at BCI and to interannual variation associated with ENSO (Detto et al. 2018). Although LM3PPA-TV simulates emergent responses to seasonal changes in temperature and water availability, leaf and canopy traits are prescribed and remain constant. The strategy adopted in LM3 to represent temperate tree phenology (degree days and minimum tolerance levels, Shevliakova et al. 2009) cannot describe the constant turnover of leaves in ever-growing, tropical trees that, instead, require the implementation of dynamic leaf traits (Restrepo-Coupe et al. 2017; Xu et al. 2016). Another challenge involves the representation of the ample diversity of reproductive strategies and

the variety of factors modulating the timing of reproduction (e.g. water availability Detto et al. 2018; Wright et al. 2019).

The LM3PPA-TV model constitutes a useful tool to analyze the interacting impacts of atmospheric CO<sub>2</sub> fertilization, changing climatic conditions, and land use patterns on the dynamics of tropical forests. In particular, future analyses could address whether the high sensitivity to water availability and drought stress revealed by our analyses results in predictions of a weakened tropical forest carbon sink in the near future. The increasing pressure on tropical forests associated with changes in land use is another facet of global change that can be analyzed using ESMs (Bonan and Doney 2018). As a result of the balance between habitat loss and restoration, more than half of tropical forests are now secondary (Chazdon 2014). Such heterogeneity in forest structure demands models which are able to simulate alternative successional pathways and its pace to recovery in order to predict carbon storage potential. Land model 3 already accommodates changes in land use, disturbance and gap recovery dynamics explicitly through its tiling scheme (Shevliakova et al. 2009) and its fire module (Rabin et al. 2018). Together, these advances enable assessment of the resilience of tropical ecosystems to changes in land use. Importantly, the LM3 dynamic soil module (Milly et al. 2014) can be extended to enable the assessment of soil erosion and degradation on forest recovery, including the impact of nutrient leaching and atmospheric deposition on nitrogen and phosphorous colimitation.

#### 6.4. Conclusions

The Land Model 3 for Tropical Vegetation (LM3PPA-TV) contributes a step towards a long-term, community effort to improve the representation of land vegetation processes in ESMs. LM3PPA-TV drew on empirical knowledge gleaned from long history of extensive research on the forest of Barro Colorado Island, Panama. The model introduces realistic assumptions about tree allometric scaling to reduce biases in biomass estimates, an updated growth allocation scheme to enable a dynamic partitioning of assimilated carbon among distinct compartments, hydraulic constraints on stomatal control, and a new compartment for tree branches and branch fall dynamics to constrain tree growth and to represent fluxes associated with coarse woody debris. This strategy enabled the simulation of realistic patterns of temporal and spatial variability in tropical forests over a broad range of scales, and equipped us with a model-based tool to test the response of tropical forests to environmental stressors across the tropics. Experiments with LM3PPA-TV showed a major role for water availability in explaining large-scale variation in ecosystem properties across the tropical forest biome. These simulations also highlighted the need to

1 improve the characterization of plant responses to water limitation, incorporate multiple functional types  
2 including geographically restricted types, and to incorporate unaccounted effects associated with small  
3 scale environmental variation. The response of tropical forests to sustained threats associated with the  
4 multiple facets of global change remains highly uncertain. ESMs are emerging as an essential tool to  
5 assess tolerable stress levels and quantify how alternative emissions scenarios will impact tropical forests.  
6 LM3PPA-TV constitutes an important advance in the representation of tropical forests dynamics in ESMs.

## 7 8 7. Acknowledgements

9 The BCI forest dynamics research project was founded by Stephen P. Hubbell and Robin B. Foster, was  
10 sustained for many years by Richard Condit, and is now managed by Stuart Davies, Suzanne Lao, and  
11 Rolando Perez under the ForestGEO program of the Smithsonian Tropical Research in Panama. Numerous  
12 organizations have provided funding, principally the US National Science Foundation, and hundreds of  
13 field workers have contributed. Data on tree traits have been gathered through several dedicated projects.  
14 I. Martínez Cano was supported by the Carbon Mitigation Initiative at Princeton University.

## 8. References

- Abernethy, K., Bush, E. R., Forget, P., Mendoza, I. and Morellato, L. P. (2018), Current issues in tropical phenology: a synthesis. *Biotropica*, 50: 477-482. doi:10.1111/btp.12558
- Anderson-Teixeira, K. J., Davies, S. J., Bennett, A. C. et al. (2015) CTFs-ForestGEO: a worldwide network monitoring forests in an era of global change. *Glob Change Biol*, 21: 528-549. doi:10.1111/gcb.12712
- Anderson-Teixeira, K. J., Wang, M. M., McGarvey, J. C., Herrmann, V., Tepley, A. J., Bond-Lamberty, B. and LeBauer, D. S. (2018), ForC: a global database of forest carbon stocks and fluxes. *Ecology*, 99: 1507-1507. doi:10.1002/ecy.2229
- Banin, L., Feldpausch, T. R., Phillips, O. L., Baker, T. R., Lloyd, J., Affum-Baffoe, K., Arets, E. J., Berry, N. J., Bradford, M., Brienen, R. J., Davies, S., Drescher, M., Higuchi, N., Hilbert, D. W., Hladik, A., Iida, Y., Salim, K. A., Kassim, A. R., King, D. A., Lopez-Gonzalez, G., Metcalfe, D., Nilus, R., Peh, K. S., Reitsma, J. M., Sonké, B., Taedoumg, H., Tan, S., White, L., Wöll, H. and Lewis, S. L. (2012), Determinants of tropical forest architecture. *Global Ecology and Biogeography*, 21: 1179-1190. doi:10.1111/j.1466-8238.2012.00778.x
- Becknell, J. M., L. K. Kucek, and J. S. Powers. 2012. Aboveground biomass in mature and secondary seasonally dry tropical forests: A literature review and global synthesis. *Forest Ecology And Management* 276:88-95.
- Bohlman, S. and Pacala, S.: A forest structure model that determines crown layers and partitions growth and mortality rates for landscape-scale applications of tropical forests. *J. Ecol.*, 100, 508-518, doi:10.1111/j.1365-2745.2011.01935.x, 2012.
- Bonan, G. B.: Forests and climate change: Forcings, feedbacks, and the climate benefits of forests. *Science*, 320, 1444-1449, doi:10.1126/science.1155121, 2008a.
- Bonan, G. B.: *Ecological Climatology. Concepts and Applications*. 2nd Edition. Cambridge University Press, New York, 2008b.
- Bonan, G. B.: Forests, Climate, and Public Policy: A 500-Year Interdisciplinary Odyssey. *Annual Review of Ecology, Evolution, and Systematics* 47: 97-121, doi.org/10.1146/annurev-ecolsys-121415-032359, 2016.
- Bonan, G. B. and Doney, S. C. (2018) Climate, ecosystems, and planetary futures: The challenge to predict life in Earth system models. *Science* 359, 533. doi:10.1126/science.aam8328
- Botkin, D. B., Janak, J. F. and Wallis, J. R.: Some Ecological Consequences of a Computer Model of Forest Growth. *J. Ecol.*, 60, 849-872, doi:10.2307/2258570, 1972.
- Cavaleri, M. A., Reed, S. C., Smith, W. K. and Wood, T. E. (2015), Urgent need for warming experiments in tropical forests. *Glob Change Biol*, 21: 2111-2121. doi:10.1111/gcb.12860
- Chapin III, F. S., Matson, P. A., and Vitousek, P.: *Principles of terrestrial ecosystem ecology*, Springer, New York, USA, 2011.
- Chave, J., Réjou-Méchain, M., Búrquez, A., Chidumayo, E., Colgan, M. S., Delitti, W. B.C., Duque, A., Eid, T., Fearnside, P. M., Goodman, R. C., Henry, M., Martínez-Yrizar, A., Mugasha, W. A., Muller-Landau, H. C., Mencuccini, M., Nelson, B. W., Ngomanda, A., Nogueira, E. M., Ortiz-Malavassi, E., Péliissier, R., Ploton, P., Ryan, C. M., Saldarriaga, J. G., and Vieilledent, G.: Improved allometric models to

- 1 estimate the aboveground biomass of tropical trees. *Glob. Change Biol.*, 20, 3177–3190,  
2 doi:10.1111/gcb.12629, 2014.
- 3 Chazdon, R. *Second Growth: The Promise of Tropical Forest Regeneration in an Age of Deforestation*. By  
4 Robin L. University of Chicago Press, Chicago, IL, USA, 472 pages. ISBN: 9780226118079, 2014.
- 5 Clark, D. B., P. C. Olivas, S. F. Oberbauer, D. A. Clark, and M. G. Ryan. 2008. First direct landscape-scale  
6 measurement of tropical rain forest Leaf Area Index, a key driver of global primary productivity.  
7 *Ecology Letters* 11:163–172, doi: 10.1111/j.1461-0248.2007.01134.x
- 8 Condit, R.: Ecological Implications of Changes in Drought Patterns: Shifts in Forest Composition in  
9 Panama, *Clim. Change*, 39, 413–427, 10.1023/a:1005395806800, 1998.
- 10 Detto, M., Asner, G. P., Muller-Landau, H. C., and Sonnentag, O. (2015), Spatial variability in tropical forest  
11 leaf area density from multireturn lidar and modeling. *J. Geophys. Res. Biogeosci.*, 120: 294– 309.  
12 doi: 10.1002/2014JG002774.
- 13 Detto, M., Wright, S. J., Calderón, O., Muller-Landau, H. C. (2018) Resource acquisition and reproductive  
14 strategies of tropical forest in response to the El Niño–Southern Oscillation. *Nature*  
15 *Communications* 9:013. <https://doi.org/10.1038/s41467-018-03306-9>
- 16 Drijfhout S, Bathiany S, Beaulieu C, Brovkin V, Claussen M, Huntingford C, Scheffer M, Sgubin G,  
17 Swingedouw D. Catalogue of abrupt shifts in Intergovernmental Panel on Climate Change climate  
18 models. *Proc Natl Acad Sci USA* 112:E5777–E5786. doi:10.1073/pnas.1511451112, 2015.
- 19 Falster, D. S., et al. (2015), BAAD: a Biomass and allometry database for woody plants. *Ecology*, 96: 1445–  
20 1445. doi:10.1890/14-1889.1
- 21 Fang, H., Baret, F., Plummer, S., & Schaepman-Strub, G. (2019). An overview of global leaf area index (LAI):  
22 Methods, products, validation, and applications. *Reviews of Geophysics*, 57.  
23 <https://doi.org/10.1029/2018RG000608>
- 24 Farrior, C. E., Bohlman, S. A., Hubbell, S., and Pacala, S. W.: Dominance of the Suppressed: Power-Law Size  
25 Structure in Tropical Forests. *Science*, 351, 155–57, doi:10.1126/science.aad0592, 2016.
- 26 Feldpausch, T. R., Banin, L., Phillips, O. L., et al.: Height-diameter allometry of tropical forest trees,  
27 *Biogeosciences*, 8, 1081–1106, 10.5194/bg-8-1081-2011, 2011
- 28 Fisher RA, Koven CD, Anderegg WRL, et al. (2018) Vegetation demographics in Earth System Models: A  
29 review of progress and priorities. *Glob Change Biol.* 24:35–54. doi: 10.1111/gcb.13910
- 30 Friedlingstein, P., M. Meinshausen, V.K. Arora, C.D. Jones, A. Anav, S.K. Liddicoat, and R. Knutti, 2014:  
31 Uncertainties in CMIP5 Climate Projections due to Carbon Cycle Feedbacks. *J. Climate*, 27, 511–  
32 526, doi.org/10.1175/JCLI-D-12-00579.1
- 33 Fyllas, N. M., L. P. Bentley, A. Shenkin, G. P. Asner, O. K. Atkin, S. Diaz, B. J. Enquist, W. Farfan-Rios, E. Gloor,  
34 R. Guerrieri, W. H. Huasco, Y. Ishida, R. E. Martin, P. Meir, O. Phillips, N. Salinas, M. Silman, L. K.  
35 Weerasinghe, J. Zaragoza-Castells, and Y. Malhi. 2017. Solar radiation and functional traits explain  
36 the decline of forest primary productivity along a tropical elevation gradient. *Ecol Lett.*
- 37 Gora, E.M., Kneale, R.C., Larjavaara, M., Muller-Landau, H.C. 2009. Dead Wood Necromass in a Moist  
38 Tropical Forest: Stocks, Fluxes, and Spatiotemporal Variability. *Ecosystems* 22: 1189.  
39 <https://doi.org/10.1007/s10021-019-00341-5>
- 40 Hubbell, S. P., Foster, R. B., O'Brien, S. T., Harms, K. E., Condit, R., Wechsler, B., et al.: Light-Gap  
41 Disturbances, Recruitment Limitation, and Tree Diversity in a Neotropical Forest, *Science*, 283,  
42 554–557, 10.1126/science.283.5401.554, 1999.

- 1 Hubbell, S. P., Condit, R., and Foster, R. B.: Barro Colorado Forest Census Plot Data  
2 <http://ctfs.si.edu/webatlas/datasets/bci>, access: Jan 20th, 2018, 2005.
- 3 Hurtt, G.C., Chini, L.P., Frolking, S. et al. (2011) Harmonization of land-use scenarios for the period 1500–  
4 2100: 600 years of global gridded annual land-use transitions, wood harvest, and resulting  
5 secondary lands. *Clim. Change* 109, 117–161. doi.org/10.1007/s10584-011-0153-2
- 6 Ingwell, L. L., S. J. Wright, K. K. Becklund, S. P. Hubbell, and S. A. Schnitzer. 2010. The impact of lianas on 10  
7 years of tree growth and mortality on Barro Colorado Island, Panama. *Journal Of Ecology* 98:879–  
8 887.
- 9 Kalnay, E., M. Kanamitsu, R. Kistler et al., 1996: The NCEP/NCAR 40-Year Reanalysis Project. *Bull. Amer.*  
10 *Meteor. Soc.*, 77, 437–472, doi.org/10.1175/1520-0477(1996)077<0437:TNYRP>2.0.CO;2
- 11 Kitajima K, Mulkey SS, Wright SJ. Variation in crown light utilization characteristics among tropical canopy  
12 trees. *Ann Bot.*, 95:535-547, 2005.
- 13 Koven, C. D., Knox, R. G., Fisher, R. A., Chambers, J., Christoffersen, B. O., Davies, S. J., Detto, M., Dietze, M.  
14 C., Faybishenko, B., Holm, J., Huang, M., Kovenock, M., Kueppers, L. M., Lemieux, G., Massoud, E.,  
15 McDowell, N. G., Muller-Landau, H. C., Needham, J. F., Norby, R. J., Powell, T., Rogers, A., Serbin, S.  
16 P., Shuman, J. K., Swann, A. L. S., Varadharajan, C., Walker, A. P., Wright, S. J., and Xu, C.:  
17 Benchmarking and Parameter Sensitivity of Physiological and Vegetation Dynamics using the  
18 Functionally Assembled Terrestrial Ecosystem Simulator (FATES) at Barro Colorado Island, Panama,  
19 *Biogeosciences Discuss.*, <https://doi.org/10.5194/bg-2019-409>, in review, 2019.
- 20 Lawrence D. and Vandecar, K. Effects of tropical deforestation on climate and agriculture. *Nature*  
21 *Climate Change* 5, 27–36, doi.org/10.1038/nclimate2430, 2015.
- 22 Le Quéré, C., Andrew, R. M., Friedlingstein, P., et al.: Global Carbon Budget 2018, *Earth Syst. Sci. Data*, 10,  
23 2141-2194, doi.org/10.5194/essd-10-2141-2018, 2018.
- 24 Leigh, E. G. *Tropical forest ecology: A view from Barro Colorado Island*. Oxford University Press, 1999.
- 25 Levine NM, Zhang K, Longo M. et al. 2016. Ecosystem heterogeneity determines the ecological resilience  
26 of the Amazon to climate change. *Proc. Natl Acad. Sci. USA* 113:793–797.  
27 doi.org/10.1073/pnas.1511344112
- 28 Lewis, S. L., B. Sonke, T. Sunderland, et al. 2013. Above-ground biomass and structure of 260 African  
29 tropical forests. *Philosophical Transactions of the Royal Society B-Biological Sciences* 368.
- 30 Lloyd, J., T. F. Domingues, F. Schrodte, F. Y. Ishida, T. R. Feldpausch, G. Saiz, C. A. Quesada, M. Schwarz, M.  
31 Torello-Raventos, M. Gilpin, B. S. Marimon, B. H. Marimon, J. A. Ratter, J. Grace, G. B. Nardoto, E.  
32 Veenendaal, L. Arroyo, D. Villarreal, T. J. Killeen, M. Steininger, and O. L. Phillips. 2015. Edaphic,  
33 structural and physiological contrasts across Amazon Basin forest-savanna ecotones suggest a  
34 role for potassium as a key modulator of tropical woody vegetation structure and function.  
35 *Biogeosciences* 12:6529-6571.
- 36 Longo, M., R. G. Knox, D. M. Medvigy, N. M. Levine, M. C. Dietze, Y. Kim, A. L. S. Swann, K. Zhang, C. R.  
37 Rollinson, R. L. Bras, S. C. Wofsy, and P. R. Moorcroft. 2019a. The biophysics, ecology, and  
38 biogeochemistry of functionally diverse, vertically and horizontally heterogeneous ecosystems:  
39 the Ecosystem Demography model, version 2.2 – Part 1: Model description. *Geosci. Model Dev.*  
40 12:4309-4346.
- 41 Longo, M., R. G. Knox, N. M. Levine, A. L. S. Swann, D. M. Medvigy, M. C. Dietze, Y. Kim, K. Zhang, D. Bonal,  
42 B. Burban, P. B. Camargo, M. N. Hayek, S. R. Saleska, R. da Silva, R. L. Bras, S. C. Wofsy, and P. R.

- Moorcroft. 2019b. The biophysics, ecology, and biogeochemistry of functionally diverse, vertically and horizontally heterogeneous ecosystems: the Ecosystem Demography model, version 2.2 – Part 2: Model evaluation for tropical South America. *Geosci. Model Dev.* 12:4347–4374.
- Malhi, Y., Farfán Amézquita, F., Doughty, C.E., et al. 2014. The productivity, metabolism and carbon cycle of two lowland tropical forest plots in south-western Amazonia, Peru. *Plant Ecology & Diversity* 7:85–105. <https://doi.org/10.1080/17550874.2013.820805>
- Maréchaux, I. and Chave, J. (2017), An individual-based forest model to jointly simulate carbon and tree diversity in Amazonia: description and applications. *Ecol Monogr*, 87: 632–664. doi:10.1002/ecm.1271
- Marvin DC, Asner GP. 2016. Branchfall dominates annual carbon flux across lowland Amazonian forests. *Environmental Research Letters* 11:094027. doi:10.1088/1748-9326/11/9/094027
- Martínez Cano I, Muller-Landau HC, Wright SJ, Bohlman SA, and Pacala SW (2019) Tropical tree height and crown allometries for the Barro Colorado Nature Monument, Panama: a comparison of alternative hierarchical models incorporating interspecific variation in relation to life history traits. *Biogeosciences* 16: 1–16, DOI:10.5194/bg-16-1-2019
- McDowell, N. , Allen, C. D., Anderson-Teixeira, K. , Brando, P. , Brien, R. , Chambers, J. , Christoffersen, B. , Davies, S. , Doughty, C. , Duque, A. , Espirito-Santo, F. , Fisher, R. , Fontes, C. G., Galbraith, D. , Goodsman, D. , Grossiord, C. , Hartmann, H. , Holm, J. , Johnson, D. J., Kassim, A. R., Keller, M. , Koven, C. , Kueppers, L. , Kumagai, T. , Malhi, Y. , McMahon, S. M., Mencuccini, M. , Meir, P. , Moorcroft, P. , Muller-Landau, H. C., Phillips, O. L., Powell, T. , Sierra, C. A., Sperry, J. , Warren, J. , Xu, C. and Xu, X. (2018), Drivers and mechanisms of tree mortality in moist tropical forests. *New Phytol*, 219: 851–869. doi:10.1111/nph.15027
- McPhaden, M. J., Zebiak, S. E., and Glantz, M. H.: ENSO as an integrating concept in Earth science, *Science*, 314, 1740–1745, doi:10.1126/science.1132588, 2006
- Meakem, V., A. J. Tepley, E. B. Gonzalez-Akre, V. Herrmann, H. C. Muller-Landau, S. J. Wright, S. P. Hubbell, R. Condit, and K. J. Anderson-Teixeira. 2018. Role of tree size in moist tropical forest carbon cycling and water deficit responses. *New Phytologist* 219:947–958.
- Meinzer et al. 2001. Regulation of water flux through tropical forest canopy trees: Do universal rules apply? *Tree Physiology* 21, 19–26
- Milly, P. C. D., Malyshev, S. L., Shevliakova, E., Dunne, K. A., Findell, K. L., Gleeson, T., Liang, Z., Phillips, P., Stouffer, R. J., and Swenson, S.: An enhanced model of land water and energy for global hydrologic and earth-system studies, *J. Hydrometeorol.*, 15, 1739–1761, doi:10.1175/JHM-D-13-0162.1, 2014
- Moorcroft, P. R., Hurtt, G. C. and Pacala, S. W. (2001), A method for scaling vegetation dynamics: the Ecosystem Demography Model (ED). *Ecological Monographs*, 71: 557–586. doi:10.1890/0012-9615(2001)071[0557:AMFSVD]2.0.CO;2
- Mora, D. Y., Jiménez, J. U. and Fábrega, J. Relación Entre el Índice de Área Foliar y el Índice Normalizado de Vegetación en el Bosque Húmedo Tropical de Panamá en Gamboa. *RIDTEC*, 10:28–40, 2014.
- Muller-Landau, H. C., Condit, R. S., Harms, K. E., Marks, C. O., Thomas, S. C., Bunyavejchewin, S., Chuyong, G., Co, L., Davies, S., Foster, R., Gunatilleke, S., Gunatilleke, N., Hart, T., Hubbell, S. P., Itoh, A., Kassim, A. R., Kenfack, D. , LaFrankie, J. V., Lagunzad, D. , Lee, H. S., Losos, E. , Makana, J. , Ohkubo, T., Samper, C., Sukumar, R., Sun, I., Nur Supardi, M. N., Tan, S., Thomas, D., Thompson, J., Valencia,

- R., Vallejo, M. I., Muñoz, G. V., Yamakura, T., Zimmerman, J. K., Dattaraja, H. S., Esufali, S., Hall, P., He, F., Hernandez, C., Kiratiprayoon, S., Suresh, H. S., Wills, C. and Ashton, P. (2006), Comparing tropical forest tree size distributions with the predictions of metabolic ecology and equilibrium models. *Ecology Letters*, 9: 589-602. doi:10.1111/j.1461-0248.2006.00915.x
- Muscarella, R., Kolyaie, S., Morton, DC, Zimmerman, JK, Uriarte, M. Effects of topography on tropical forest structure depend on climate context. *J Ecol.* 2019; 00: 1– 15. <https://doi.org/10.1111/1365-2745.13261>
- Pacala, S. W., Canham, C. D., Saponara, J., Silander, J. A., Kobe, R. K., and Ribbens, E.: Forest models defined by field measurements: estimation, error analysis and dynamics. *Ecol. Monogr.*, 66, 1–43, 1996.
- Palace, M., M. Keller, and H. Silva. 2008. Necromass production: Studies in undisturbed and logged Amazon forests. *Ecological Applications* 18:873-884.
- Pan, Y., R. A. Birdsey, O. L. Phillips, and R. B. Jackson. 2013. The structure, distribution, and biomass of the world's forests. *Annual Review of Ecology, Evolution, and Systematics* 44:1, 593-622.
- Powell, T. L., Koven, C. D., Johnson, D. J., Faybishenko, B., Fisher, R. A., Knox, R. , McDowell, N. G., Condit, R., Hubbell, S. P., Wright, S. J., Chambers, J. and Kueppers, L. M. (2018), Variation in hydroclimate sustains tropical forest biomass and promotes functional diversity. *New Phytol*, 219: 932-946. doi:10.1111/nph.15271
- Prentice, I. C., Cramer, W., Harrison, S. P., et al.: A global biome model based on plant physiology and dominance, soil properties and climate, *J Biogeogr*, 19, 117-134, citeulike-article-id:1309692, 1992.
- Purves, D. W., Lichstein, J. W., Strigul, N., and Pacala, S. W. Predicting and understanding forest dynamics using a simple tractable model. *PNAS*, 105 (44) 17018-17022. doi: 10.1073/pnas.0807754105, 2008.
- Rabin, S. S., Ward, D. S., Malyshev, S. L., Magi, B. I., Shevliakova, E. and Pacala, S. W. A fire model with distinct crop, pasture, and non-agricultural burning: use of new data and a model-fitting algorithm for FINAL1. *Geoscientific Model Development* 11: 815-842, doi: 10.5194/gmd-11-815-2018, 2018.
- Restrepo-Coupe, N. , Levine, N. M., Christoffersen, B. O., Albert, L. P., Wu, J. , Costa, M. H., Galbraith, D. , Imbuzeiro, H. , Martins, G. , Araujo, A. C., Malhi, Y. S., Zeng, X. , Moorcroft, P. and Saleska, S. R. (2017), Do dynamic global vegetation models capture the seasonality of carbon fluxes in the Amazon basin? A data-model intercomparison. *Glob Change Biol*, 23: 191-208. doi:10.1111/gcb.13442
- Running, S., Mu, Q., Zhao, M. (2015). MOD17A3H MODIS/Terra Net Primary Production Yearly L4 Global 500m SIN Grid V006 [Data set]. NASA EOSDIS Land Processes DAAC. doi:10.5067/MODIS/MOD17A3H.006
- Rutishauser E, Wright SJ, Condit R, Hubbell SP, Davies SJ, Muller-Landau HC (2020) Testing for changes in biomass dynamics in large-scale forest datasets. *Global Change Biology*, 26, 1485-1498. <https://doi.org/10.1111/gcb.14833>
- Sakai, S, Kitajima, K. Tropical phenology: Recent advances and perspectives. *Ecol. Res.* 2019; 34: 50– 54. <https://doi.org/10.1111/1440-1703.1131>
- Schimel, D., Stephens, B.B. & Fisher, J.B. (2014), Effect of increasing CO<sub>2</sub> on the terrestrial carbon cycle. *Proc. Natl. Acad. Sci.*, 112, 201407302. <https://doi.org/10.1073/pnas.1407302112>

- Schimel, D. , Pavlick, R. , Fisher, J. B., Asner, G. P., Saatchi, S. , Townsend, P. , Miller, C. , Frankenberg, C. ,  
Hibbard, K. and Cox, P. (2015), Observing terrestrial ecosystems and the carbon cycle from space.  
Glob Change Biol, 21: 1762-1776. doi:10.1111/gcb.12822
- Sheffield, J., Goteti, G., and Wood, E. F.: Development of a 50-year high-resolution global dataset of  
meteorological forcings for land surface modeling, J. Climate, 19, 3088–3111,  
doi:10.1175/Jcli3790.1, 2006.
- Shevliakova, E., S. W. Pacala, S. Malyshev, G. C. Hurtt, P. C. D. Milly, J. P. Caspersen, L. T. Sentman, J. P. Fisk,  
C. Wirth, and C. Crevoisier (2009), Carbon cycling under 300 years of land use change: Importance  
of the secondary vegetation sink, Global Biogeochem. Cycles, 23, GB2022,  
doi:10.1029/2007GB003176.
- Shugart, H. H. and West, D. C.: Development of an Appalachian deciduous forest succession model and its  
application to assessment of the impact of the chestnut blight, J. Environ. Manage., 5, 161–179,  
1977.
- Slik, J. W. F., J. Franklin, V. Arroyo-Rodriguez et al. 2018. Phylogenetic classification of the world's tropical  
forests. Proceedings Of The National Academy Of Sciences Of The United States Of America  
115:1837-1842.
- Snyder, P.K., 2010: The Influence of Tropical Deforestation on the Northern Hemisphere Climate by  
Atmospheric Teleconnections. Earth Interact., 14, 1–34, <https://doi.org/10.1175/2010EI280.1>
- Strigul, N., Pristinski, D., Purves, D., Dushoff, J. and Pacala, S. (2008), SCALING FROM TREES TO FORESTS:  
TRACTABLE MACROSCOPIC EQUATIONS FOR FOREST DYNAMICS. Ecological Monographs, 78:  
523–545. doi:10.1890/08-0082.1
- Sulman, B. N., Shevliakova, E., Brzostek, E. R., Kivlin, S. N., Malyshev, S., Menge, D. N. L., & Zhang, X. (2019).  
Diverse mycorrhizal associations enhance terrestrial C storage in a global model. Global  
Biogeochemical Cycles, 33, 501– 523. <https://doi.org/10.1029/2018GB005973>
- Taylor, P. G., Cleveland, C. C., Soper, F., Wieder, W. R., Dobrowski, S. Z., Doughty, C. E., and Townsend, A. R.  
2019. Greater stem growth, woody allocation, and aboveground biomass in Paleotropical forests  
than in Neotropical forests. Ecology 100(3):e02589. 10.1002/ecy.2589
- Vilanova, E., H. Ramirez-Angulo, A. Torres-Lezama, G. Aymard, L. Gamez, C. Duran, L. Hernandez, R.  
Herrera, G. van der Heijden, O. L. Phillips, and G. J. Etal. 2018. Environmental drivers of forest  
structure and stem turnover across Venezuelan tropical forests. Plos One 13.
- Weng, E. S., S. Malyshev, J. W. Lichstein, C. E. Farrior, R. Dybzinski, T. Zhang, E. Shevliakova, and S. W.  
Pacala: Scaling from Individual Trees to Forests in an Earth System Modeling Framework Using a  
Mathematically Tractable Model of Height-Structured Competition. Biogeosciences, 12, 2655–94,  
doi:10.5194/bg-12-2655-2015, 2015.
- Weng, E., Farrior, C. E., Dybzinski, R. and Pacala, S. W.: Predicting vegetation type through physiological  
and environmental interactions with leaf traits: evergreen and deciduous forests in an earth  
system modeling framework. Glob Change Biol., 23, 2482–2498. doi:10.1111/gcb.13542, 2017.
- Wirth, R., Weber, B., Ryel, R. J. Spatial and temporal variability of canopy structure in a tropical moist  
forest. Acta Oecologica 22, 235-244, 2001, doi:10.1016/S1146-609X(01)01123-7
- Wolf, A., Anderegg, W. R. L. and Pacala, S. W. Optimal stomatal behavior with competition for water and  
risk of hydraulic impairment. Proceedings of the National Academy of Sciences, 113:E7222-E7230,  
doi: 10.1073/pnas.1615144113, 2016.

- 1 Wright, S. J., van Schaik C. P. (1994) Light and the Phenology of Tropical Trees. *The American Naturalist*  
2 143:192-199.
- 3 Wright, S. J., Kitajima, K., Kraft, N. J. B., et al.: Functional traits and the growth–mortality trade-off in  
4 tropical trees, *Ecology*, 91, 3664–3674, doi:10.1890/09-2335.1, 2010.
- 5 Wright, S. J. 2019. Plant responses to nutrient addition experiments conducted in tropical forests.  
6 *Ecological Monographs* 00(00):e01382. 10.1002/ecm.1382
- 7 Wu, J., Albert, L. P., Lopes, A. P., et al. (2016). Leaf development and demography explain photosynthetic  
8 seasonality in Amazon evergreen forests. *Science*, 351, 972–976. doi: 10.1126/science.aad5068
- 9 Wu, J., Serbin, SP, Xu, X, et al. The phenology of leaf quality and its within-canopy variation is essential for  
10 accurate modeling of photosynthesis in tropical evergreen forests. *Glob Change Biol.* 2017; 23:  
11 4814– 4827. <https://doi.org/10.1111/gcb.13725>
- 12 Wurzburger, N. and Wright, S. J. (2015), Fine-root responses to fertilization reveal multiple nutrient  
13 limitation in a lowland tropical forest. *Ecology*, 96: 2137–2146. doi:10.1890/14-1362.1
- 14 Xu, X., Medvigy, D., Powers, J. S., Becknell, J. M. and Guan, K. (2016) Diversity in plant hydraulic traits  
15 explains seasonal and inter-annual variations of vegetation dynamics in seasonally dry tropical  
16 forests. *New Phytol*, 212: 80-95. doi:10.1111/nph.14009
- 17

## 9. Figures

Figure 1. Schematic of a LM3PPA-TV land tile covered by vegetation. The model structures vegetation into distinct canopy layers that receive different amounts of light. Within each canopy layer, trees that belong to the same plant functional type are grouped into cohorts defined by tree size and density. Trees in lower layers are shaded by trees in higher layers; trees in the same layer do not shade each other. Within the canopy of individual trees, there is self-shading from higher to lower layers of leaves.

Figure 2. Time series of annual GPP and NPP generated by LM3PPA-TV monoculture experiments run in a single  $1^\circ \times 1^\circ$  cell, with climate conditions corresponding to Barro Colorado Island (BCI), Panama ( $9.5^\circ \text{N}$ ,  $9.5^\circ \text{W}$ ) (lines), in comparison with independent estimates of GPP and NPP on BCI (dots) and in other mature, intact tropical forests in the *ForC* database of Anderson-Teixeira et al. (2018) (vertical brackets). The simulation featured a single tree functional type parameterized for a shade-tolerant tropical forest canopy tree, specifically the BCI species *Beilschmiedia pendula* (see §4.1 for further details). The BCI estimate of GPP is based on eddy covariance measurements for July 2012 – August 2017 ( $2.7 \text{ kg C m}^{-2} \text{ yr}^{-1}$ ); the BCI estimate of NPP is based on the average of MODIS data for the period 2000-2014 ( $1.2 \text{ kg C m}^{-2} \text{ yr}^{-1}$ , Running et al. 2015).

Figure 3. Flow diagram showing the carbon fluxes in LM3PPA-TV simulations of the BCI forest, with band widths proportional to the flux sizes. The values shown are averages over the last 100 years of a 500-yr monoculture run (*Beilschmiedia pendula* PFT).

Figure 4. Simulated and observed diurnal cycles of gross photosynthesis [ $\mu\text{mol CO}_2 \text{ m}^{-2} \text{ s}^{-1}$ ] and evapotranspiration [ $\text{W m}^{-2}$ ] during the dry and wet seasons at BCI. The thick lines and shading represent, respectively, the median and 90% quantile intervals of LM3PPA-TV simulations. Green lines show field estimates based on eddy covariance flux measurements at BCI (continuous and dashed lines for the dry and wet seasons, respectively). For this analysis, the dry season was defined as 16 weeks starting on December 23, and the wet season as the rest of the year. Evapotranspiration integrates plant transpiration, fluxes due to the evaporation of ground water, and the evaporation of water intercepted by the vegetation during precipitation.

Figure 5. Distribution of simulated (grey bars) and observed (green bars) annual diameter growth rates [ $\text{mm yr}^{-1}$ ] for canopy and understory trees on BCI. Observed growth rates were calculated from trunk diameter increments in five-year census intervals (see section §10.4 for further details, including the classification of trees as canopy vs. understory). Simulated growth rates correspond to the distribution of the annual average rates for *Beilschmiedia pendula* canopy and understory trees during the last 100 years of a 500-yr monoculture run of LM3PPA-TV.

Figure 6. Observed (green dots) and simulated (other colors) tree size distribution (i.e., community size spectra) for BCI. Observed distributions are for main stems of all trees of all species in the 50 ha BCI

1 census plot in 2015. Simulated distributions are the averages over the last 100 years of 500-year-long  
2 monoculture runs of LM3PPA-TV parameterized with data for one of four shade-tolerant canopy tree  
3 species on BCI: *Beilschmiedia pendula*, *Brosimum alicastrum*, *Prioria copaifera*, and *Quararibea asterolepis*.  
4 Each point represents a logarithmic tree diameter bin, with tree densities expressed per area of ground  
5 and per m of tree diameter.

6  
7 Figure 7. Observed vs. simulated total tree above ground biomass (AGB, Kg C m<sup>-2</sup>) across 162 mature,  
8 intact tropical forest sites. Observed stand level AGB estimates are from the *ForC* database (Anderson-  
9 Teixeira et al. 2018). AGB predictions are based on LM3PPA-TV monoculture runs featuring the plant  
10 functional type parameterized from BCI data for the species *Beilschmiedia pendula*. Meteorological  
11 conditions were from the nearest 1°x1° cell in Sheffield et al. (2006) forcing data.

12  
13 Figure 8. Simulated (black) and observed (green) tree size distributions in nine tropical forests within the  
14 Smithsonian ForestGeo network. Simulated distributions are the averages over the last 100 years of 500-  
15 year-long monoculture runs of LM3PPA-TV parameterized with BCI data for *Beilschmiedia pendula*.  
16 Observed distributions are for trees of all species combined, as reported in Muller-Landau et al. (2006).  
17 Sites are ordered from wettest to driest.



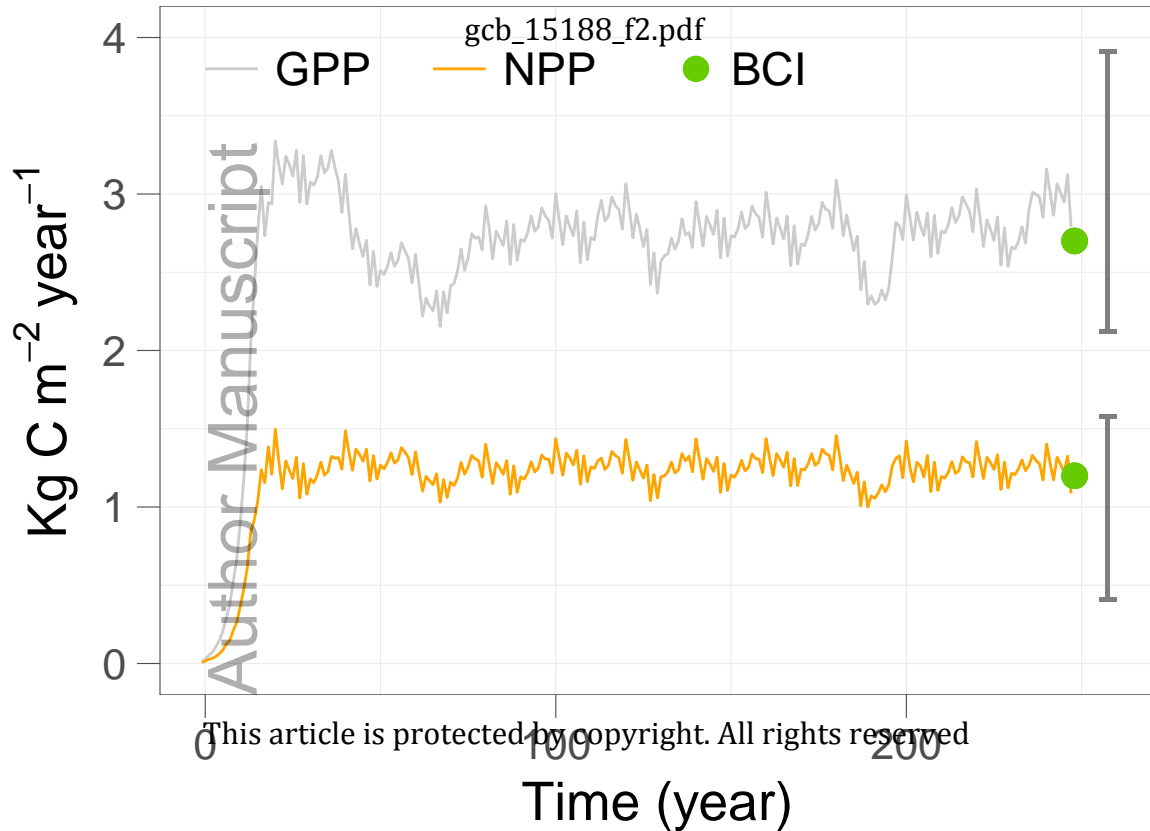
Author Manuscript

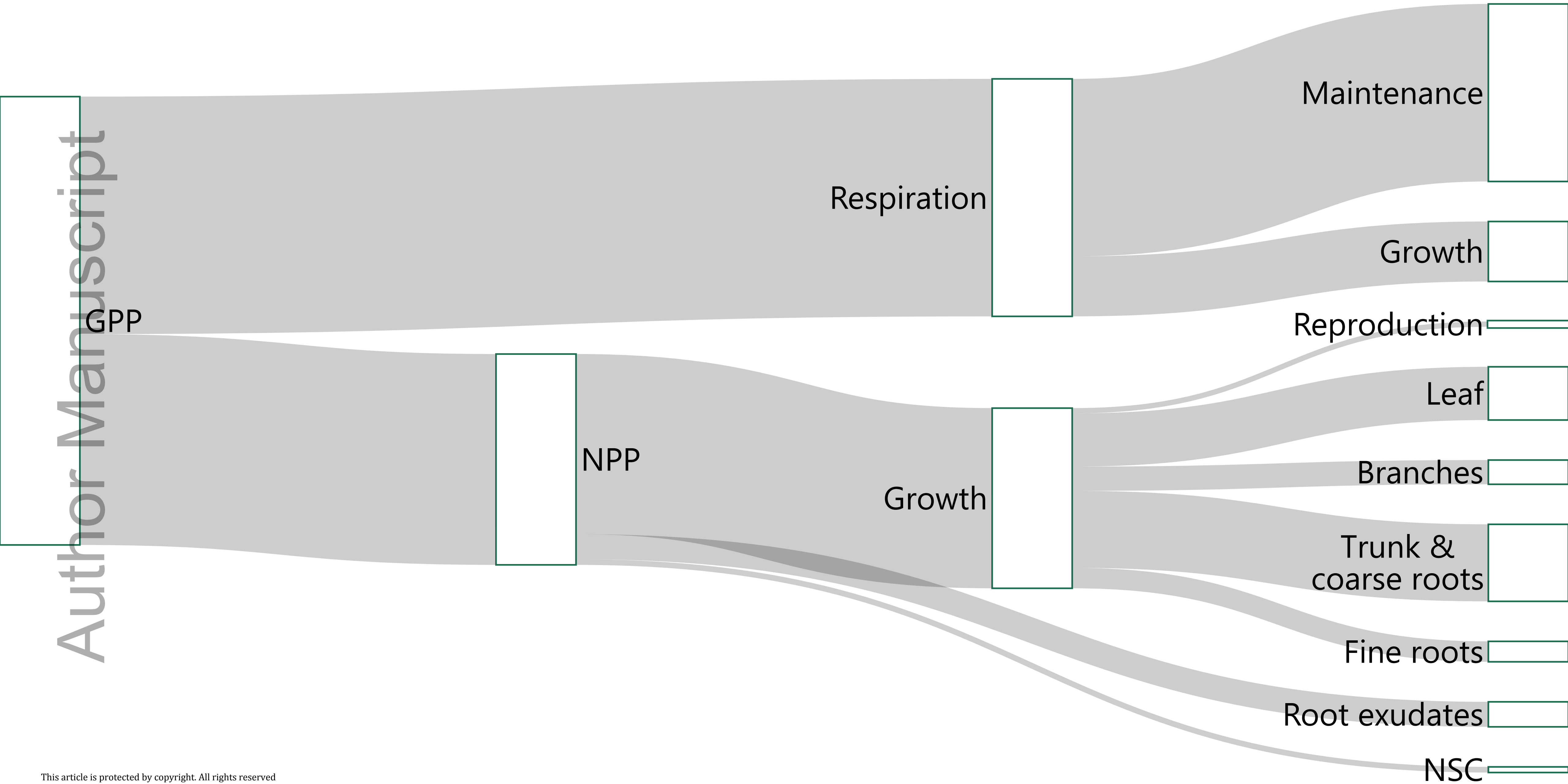
Cohort

Canopy layer

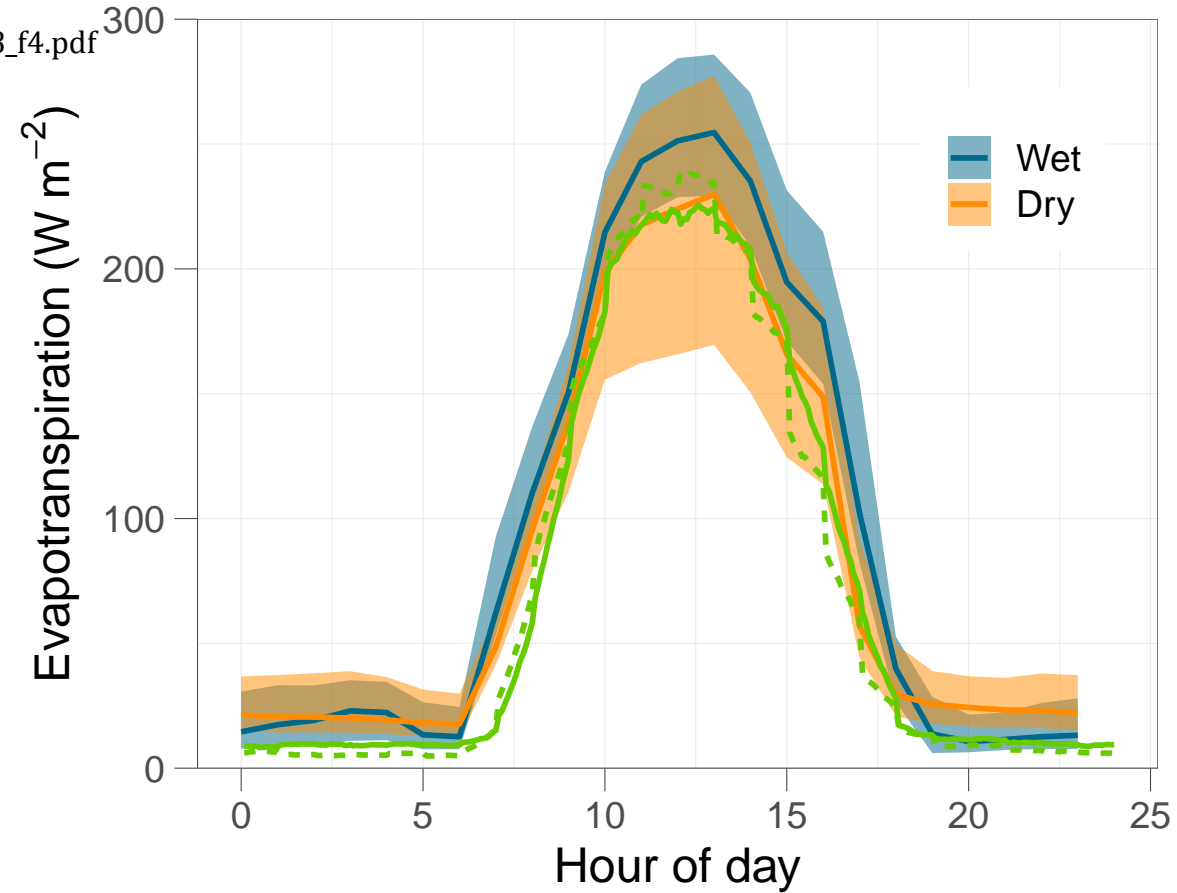
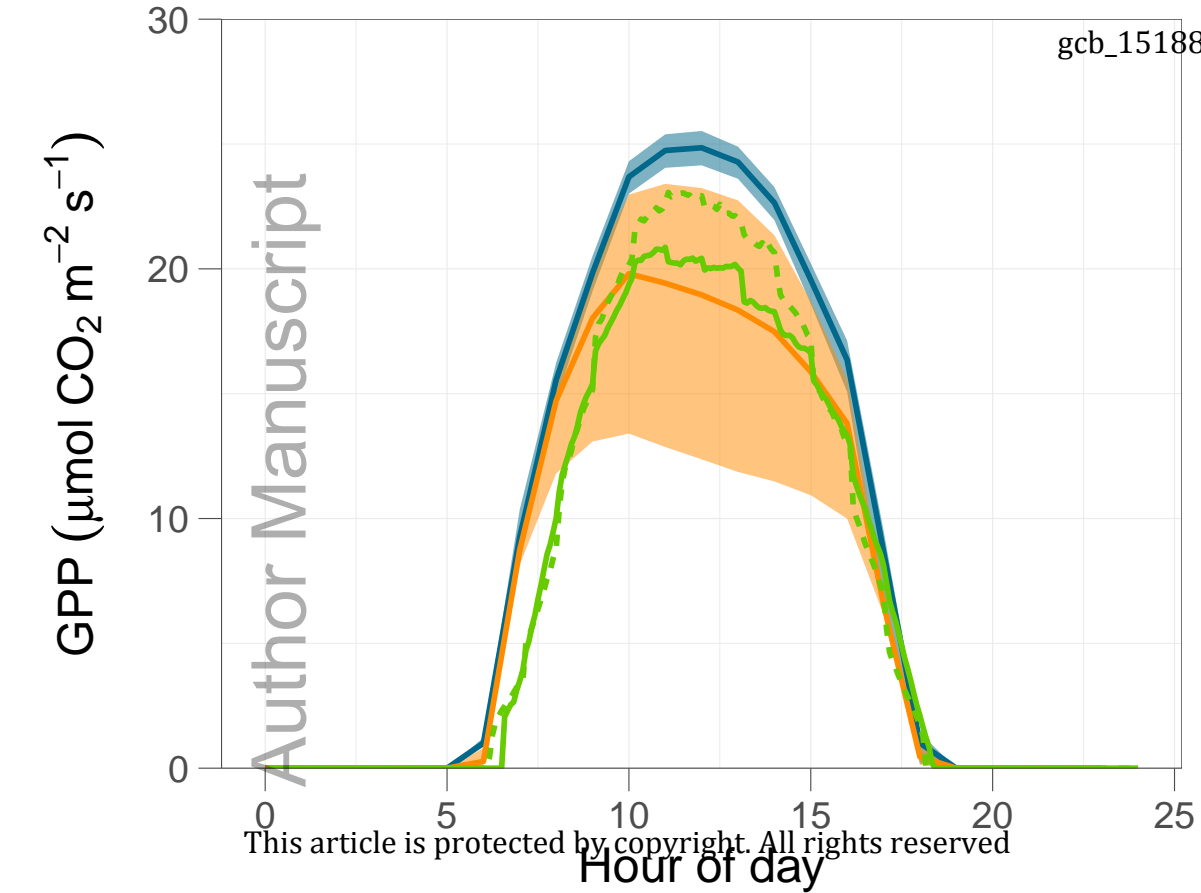
Understory layers

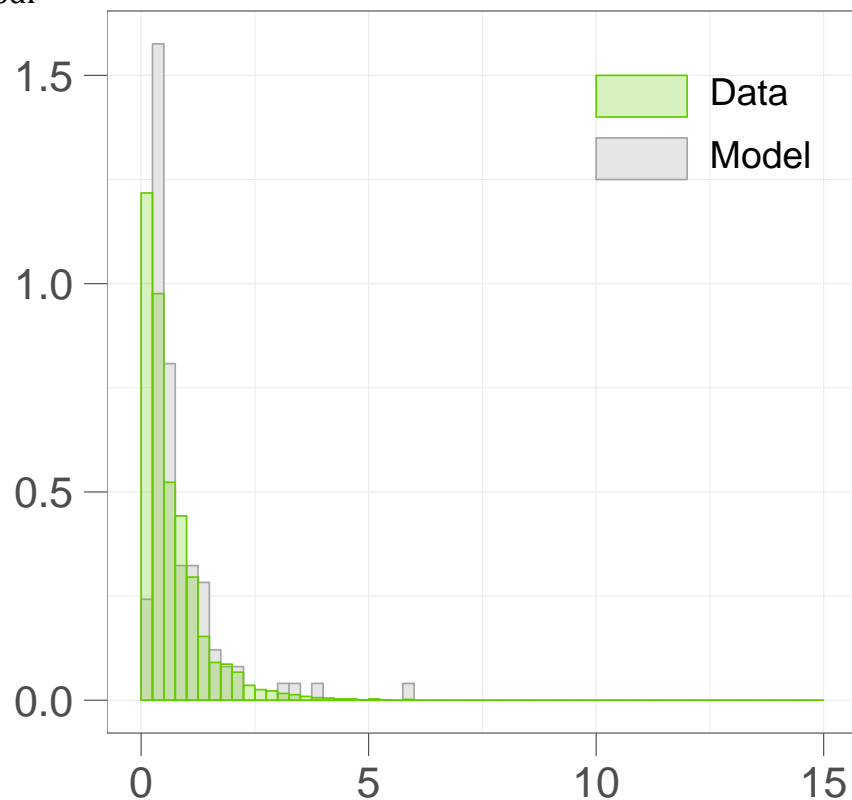
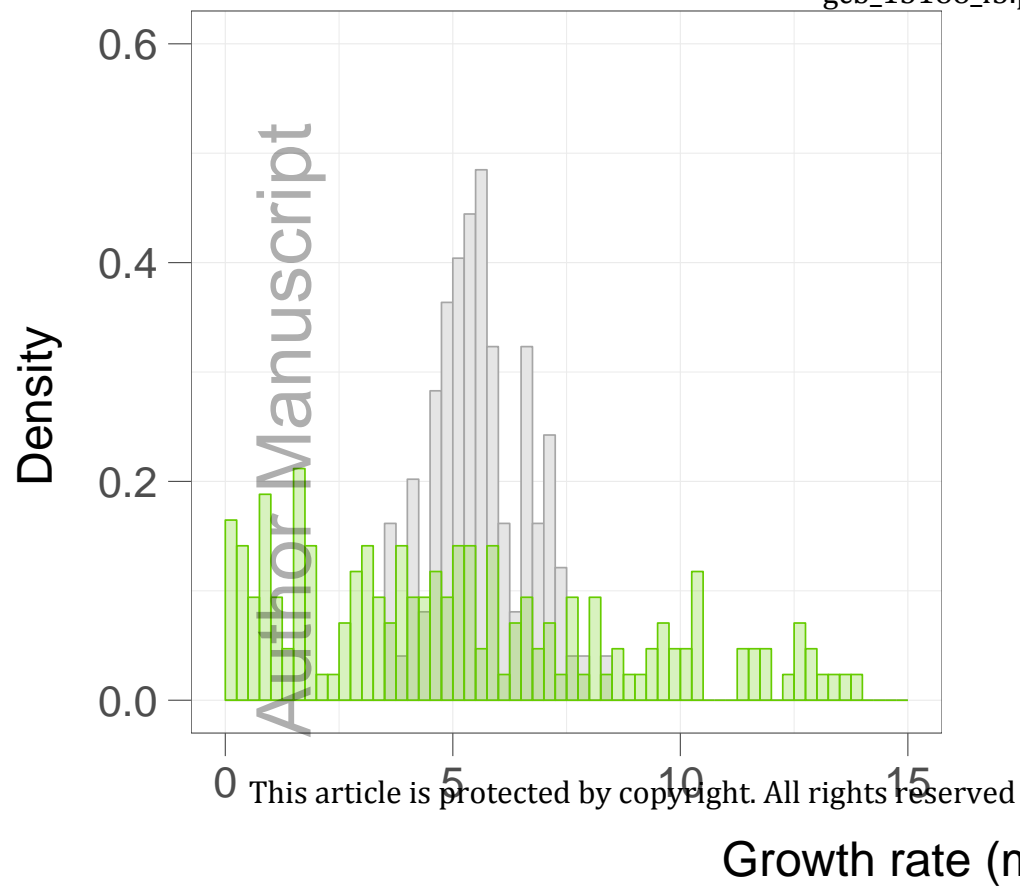
Land tile

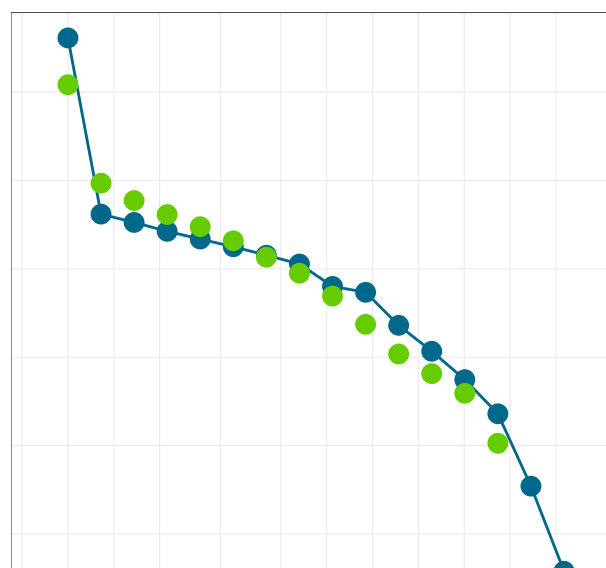
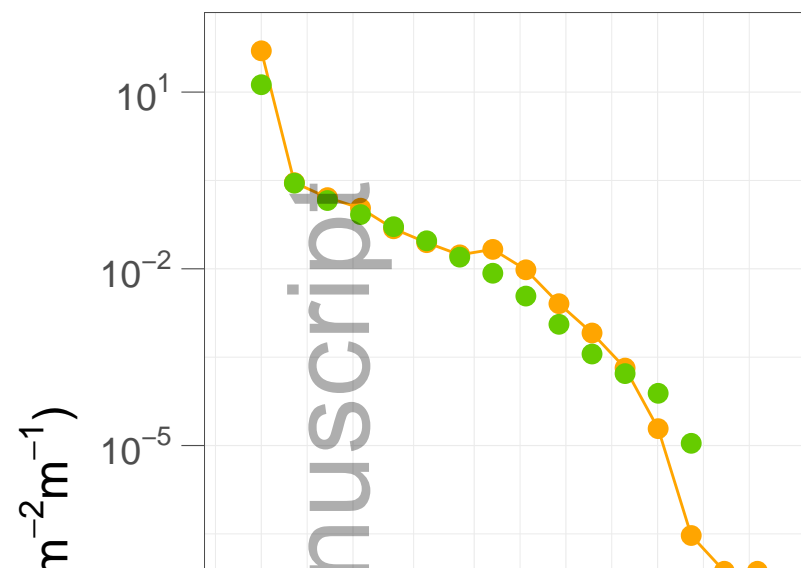
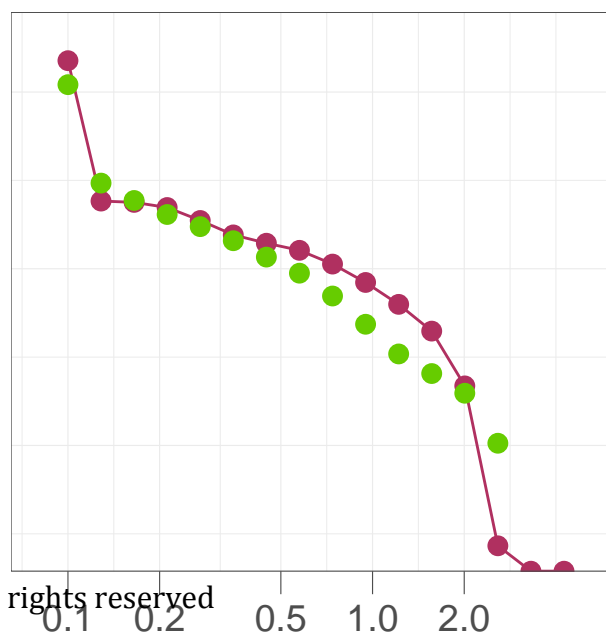
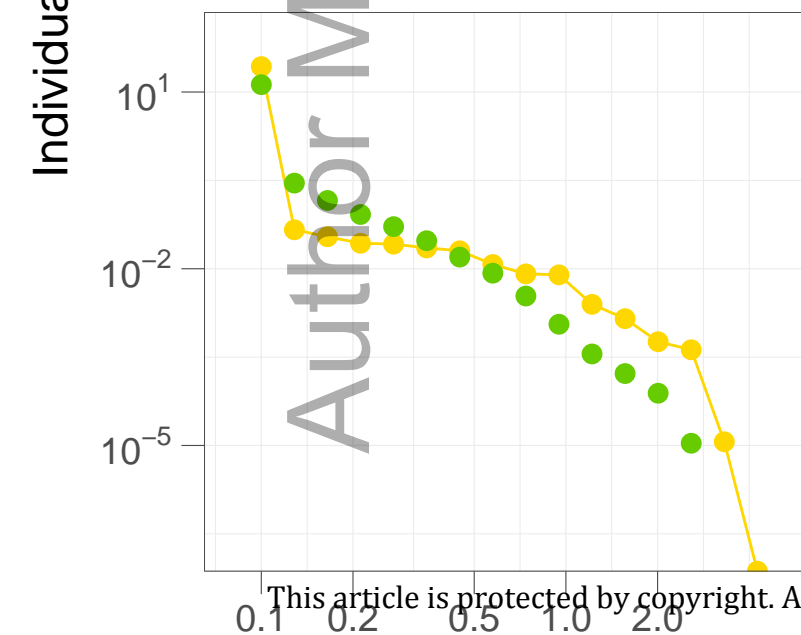




Author Manuscript

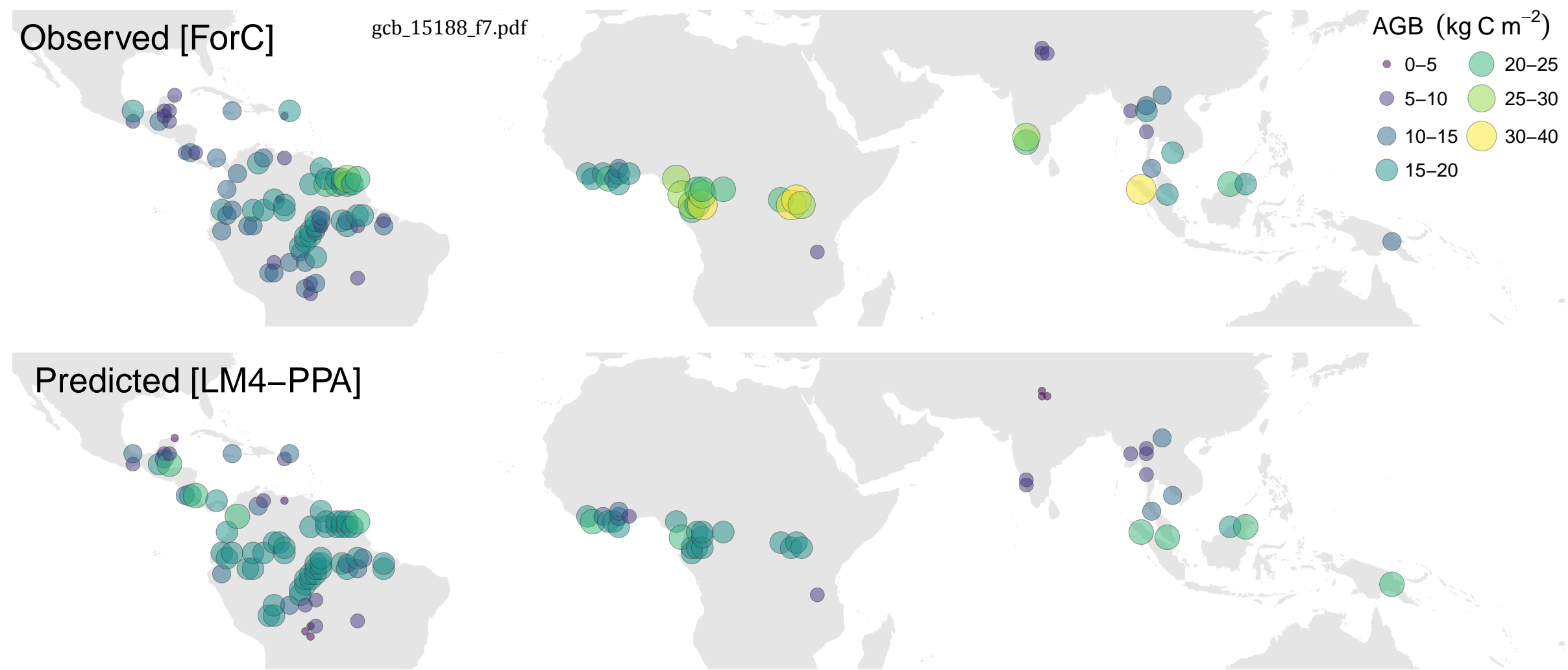
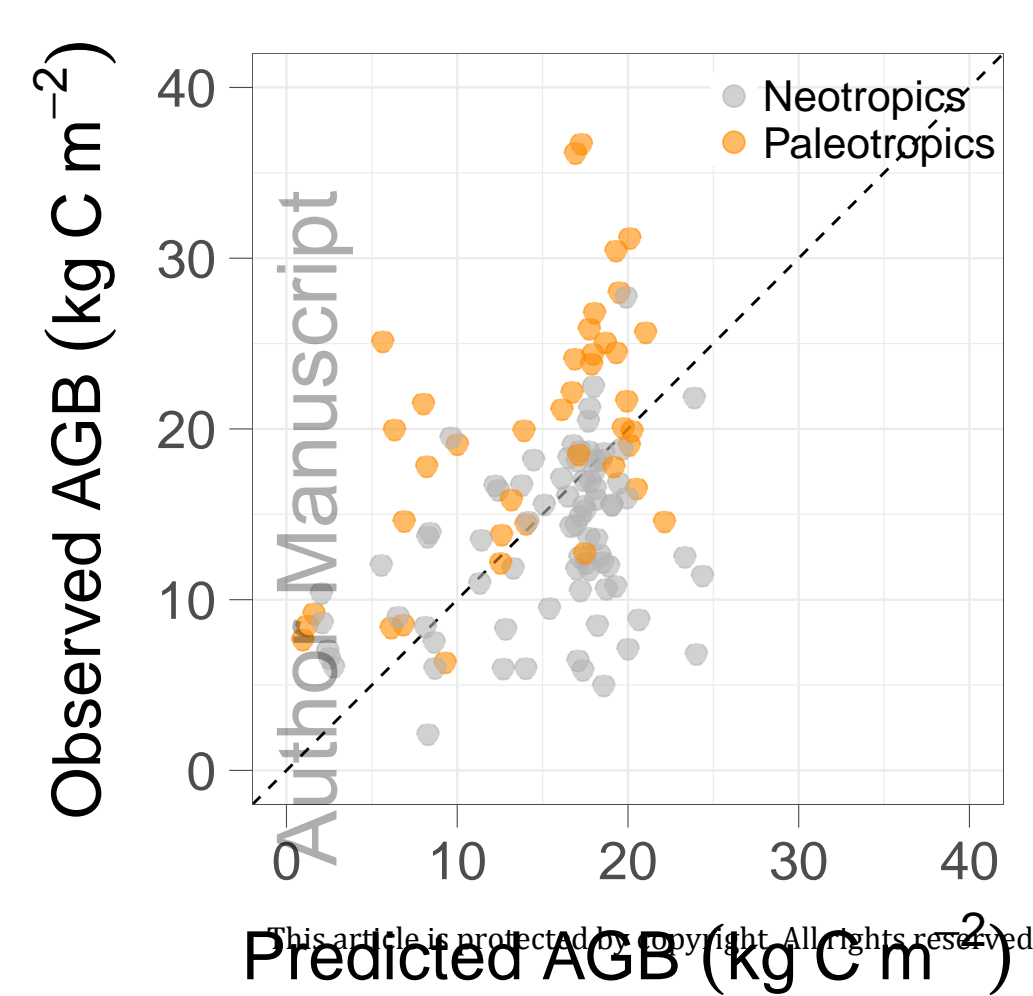


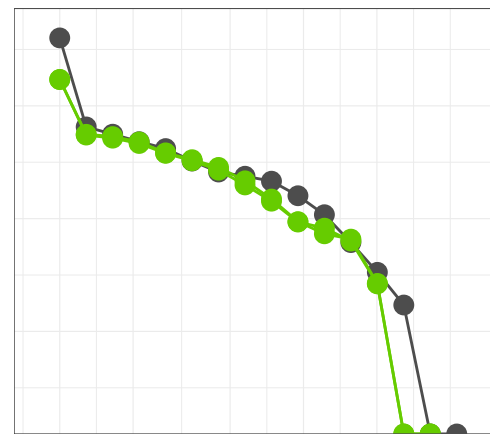
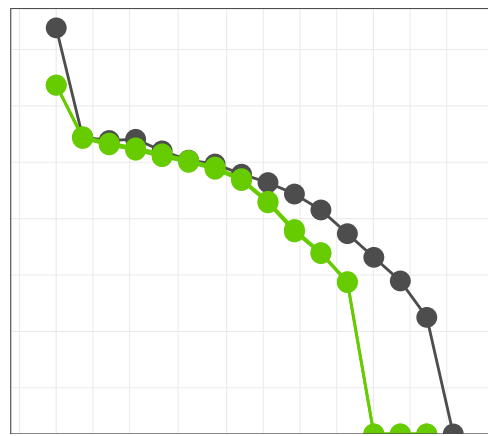
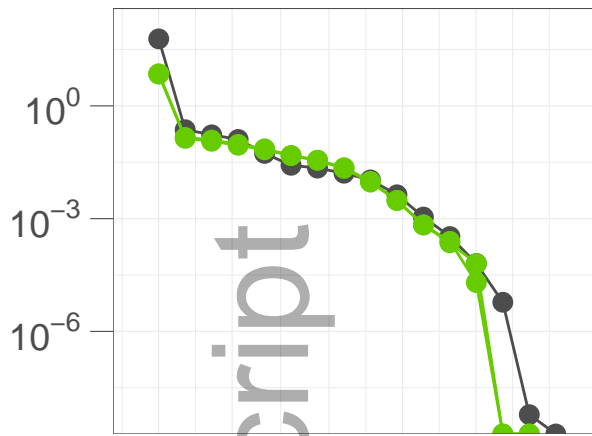
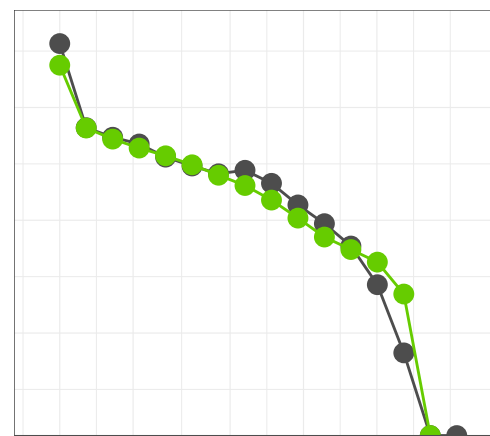
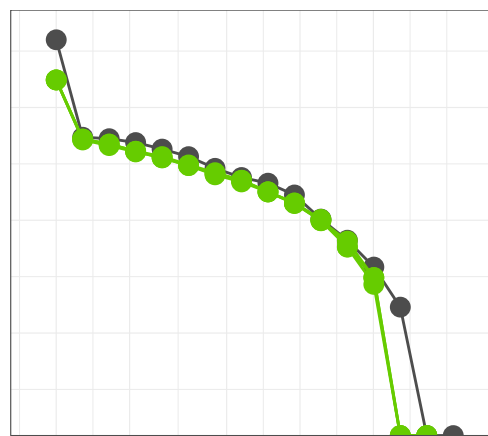
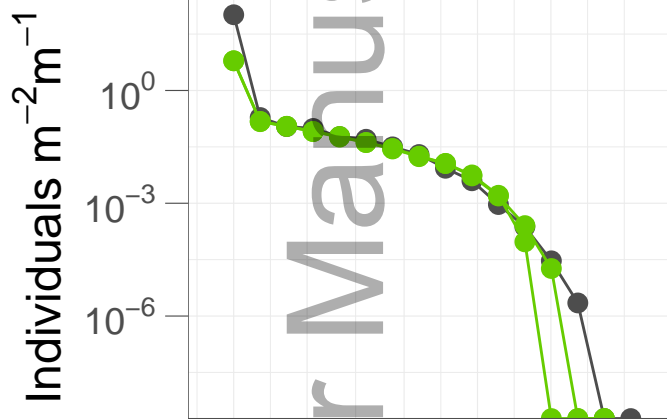
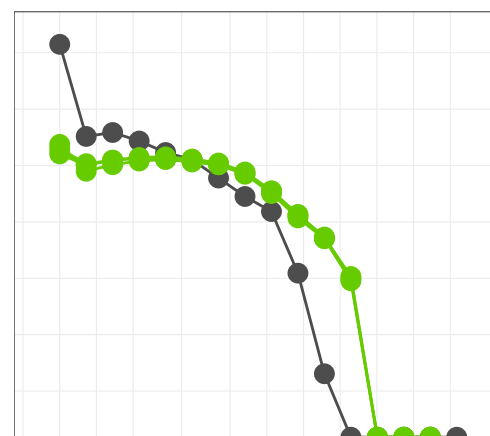
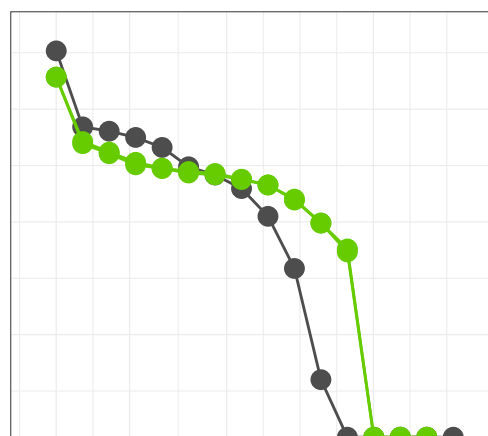
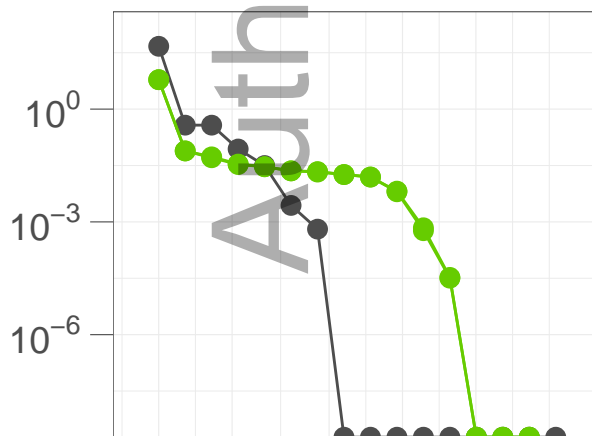


*Beilschmiedia**Brosimum**Prioria**Quararibea*

This article is protected by copyright. All rights reserved

Stem diameter (m)



*Sinharaja**La Planada**Yasuni**Lambir**Pasoh**BCI**Ituri-Lenda**Ituri-Edoro**Mudumalai*

Stem diameter (m)